

pH Regulation by NHX-Type Antiporters Is Required for Receptor-Mediated Protein Trafficking to the Vacuole in Arabidopsis

Maria Reguera,^{a,1} Elias Bassil,^{a,1} Hiromi Tajima,^a Monika Wimmer,^b Alexandra Chanoca,^c Marisa S. Otegui,^c Nadine Paris,^d and Eduardo Blumwald^{a,2}

^aDepartment of Plant Sciences, University of California, Davis, California 95616

^bInstitute of Crop Science and Resource Conservation, Division of Plant Nutrition, University of Bonn, D-53115 Bonn, Germany

^cDepartments of Botany and Genetics, University of Wisconsin, Madison, Wisconsin 53706

^dBiochemistry and Plant Molecular Biology Laboratory, Unité Mixte de Recherche 5004, 34060 Montpellier, France

Protein trafficking requires proper ion and pH homeostasis of the endomembrane system. The NHX-type Na⁺/H⁺ antiporters NHX5 and NHX6 localize to the Golgi, *trans*-Golgi network, and prevacuolar compartments and are required for growth and trafficking to the vacuole. In the *nhx5 nhx6* T-DNA insertional knockouts, the precursors of the 2S albumin and 12S globulin storage proteins accumulated and were missorted to the apoplast. Immunoelectron microscopy revealed the presence of vesicle clusters containing storage protein precursors and vacuolar sorting receptors (VSRs). Isolation and identification of complexes of VSRs with unprocessed 12S globulin by 2D blue-native PAGE/SDS-PAGE indicated that the *nhx5 nhx6* knockouts showed compromised receptor-cargo association. In vivo interaction studies using bimolecular fluorescence complementation between VSR2;1, aleurain, and 12S globulin suggested that *nhx5 nhx6* knockouts showed a significant reduction of VSR binding to both cargoes. In vivo pH measurements indicated that the lumens of VSR compartments containing aleurain, as well as the *trans*-Golgi network and prevacuolar compartments, were significantly more acidic in *nhx5 nhx6* knockouts. This work demonstrates the importance of NHX5 and NHX6 in maintaining endomembrane luminal pH and supports the notion that proper vacuolar trafficking and proteolytic processing of storage proteins require endomembrane pH homeostasis.

INTRODUCTION

The homeostatic control of ions and pH in intracellular compartments is fundamental to basic cellular processes needed to maintain normal plant growth as well as the responses to stress (Bassil and Blumwald, 2014). Intracellular pH is established by the activity of H⁺ pumps, vacuolar ATPase (V-ATPase), and pyrophosphatase in the vacuoles and v-ATPase in vesicles (Rea and Poole, 1993; Matsuoka et al., 1997; Dettmer et al., 2006), which generate the H⁺ electrochemical potential needed by secondary transporters to couple the passive transport of H⁺ to the movement of secondary ions against their electrochemical potential (Blumwald, 1987). The activity of v-ATPase alone is likely to be insufficient to establish or maintain pH, and alkalizing mechanisms are also required to achieve pH homeostasis in specific intracellular compartments (Orlowski and Grinstein, 2011; Bassil et al., 2012).

NHX-type Na⁺(K⁺)/H⁺ exchangers are particularly important for the regulation of pH and ion homeostasis and have been implicated in a wide variety of physiological processes, including cell volume and expansion, osmotic adjustment, and stress responses (Rodríguez-Rosales et al., 2009; Bassil et al., 2012). They operate

by exchanging luminal H⁺ for Na⁺ or K⁺ and, therefore, regulate monovalent cation homeostasis in addition to functioning as “H⁺ leaks” to fine-tune luminal pH by countering the acidity generated by the H⁺ pumps (Orlowski and Grinstein, 2011). *Arabidopsis thaliana* contains six intracellular NHX isoforms (Bassil et al., 2012; Chanroj et al., 2012). NHX1 to NHX4 reside on the tonoplast and are required for vacuolar pH and K⁺ homeostasis (Apse et al., 2003; Bassil et al., 2011b), salt stress responses (Apse et al., 1999), osmotic adjustment (Barragán et al., 2012), and flower development (Yoshida et al., 1995; Bassil et al., 2011b). The two remaining isoforms, NHX5 and NHX6, localize to the Golgi and *trans*-Golgi network (TGN), compartments that are sensitive to brefeldin A and wortmanin (Bassil et al., 2011a; Martinière et al., 2013). The double knockout *nhx5 nhx6* exhibited significantly reduced cell expansion and growth, severe sensitivity to salt, and defects in trafficking to the vacuole, as assessed by the missorting of transiently expressed carboxypeptidase Y to the apoplast of *Arabidopsis* cotyledon mesophyll cells and by a delay in labeling the tonoplast by the endocytotic tracer dye FM4-64 (Bassil et al., 2011a). Transcriptome analysis of *nhx5 nhx6* also revealed that a number of trafficking-related transcripts were differentially regulated as compared with wild-type plants (Bassil et al., 2011a). Some of these transcripts included those encoding the Vacuolar Sorting Receptor1 (VSR1;1), the SNARE VTI12, and a putative subunit of the retromer complex VPS35a, all of which are implicated in anterograde and retrograde trafficking in plant cells (Shimada et al., 2003; Sanmartín et al., 2007; Craddock et al., 2008; Yamazaki et al., 2008; Nodzyński et al., 2013). The localization and biochemical function of NHX5 and

¹ These authors contributed equally to this work.

² Address correspondence to eblumwald@ucdavis.edu.

The author responsible for distribution of materials integral to the findings presented in this article in accordance with the policy described in the Instructions for Authors (www.plantcell.org) is: Eduardo Blumwald (eblumwald@ucdavis.edu).

www.plantcell.org/cgi/doi/10.1105/tpc.114.135699

NHX6, and the trafficking-related phenotypes of *nhx5 nhx6*, raise key questions on the importance of endomembrane luminal pH to vesicular trafficking.

Vesicular pH is believed to be critical for the sorting of newly synthesized proteins, vesicle identity, enzyme activity, endocytosis, receptor-cargo interaction, as well as the degradation or recycling of molecules (Paroutis et al., 2004). In animal cells, the luminal pH of each intracellular compartment along the secretory pathway is progressively more acidic (Paroutis et al., 2004). Perturbations of the proteins that regulate intracellular pH lead to aberrant pH and diverse trafficking phenotypes in both animals and yeast (Casey et al., 2010; Ohgaki et al., 2011; Orłowski and Grinstein, 2011). In plants, the effect of reduced V-ATPase activity on endocytotic and secretory trafficking has suggested that pH is also important to protein trafficking (Matsuoka et al., 1997; Dettmer et al., 2006). The use of genetically encoded pH sensors that target to specific cellular compartments of the endomembrane system has allowed in vivo pH measurements of most intracellular compartments in plants (Martinière et al., 2013; Shen et al., 2013) and has been instrumental in fully understanding the role of endomembrane luminal pH in protein processing and trafficking. Studies aimed at investigating the direct role of pH-regulating mechanisms are thus now possible.

Soluble proteins, including the major Arabidopsis storage proteins 12S globulins and 2S albumins or the vacuolar thiol protease aleurain, are synthesized in the endoplasmic reticulum (ER), where they initiate their trafficking before accumulating in protein storage vacuoles (PSVs). A critical sorting step en route to the vacuole seems to occur at the TGN, where secretory and endocytic trafficking converge (Dettmer et al., 2006; Lam et al., 2007; Toyooka et al., 2009; Viotti et al., 2010; Scheuring et al., 2011), similar to what has been observed in the early endosome of animal cells. The importance of the TGN as a main sorting hub of cellular cargo has become increasingly accepted (Reyes et al., 2011; Schumacher, 2014). In plants, the selective trafficking of soluble proteins to the vacuole is mediated by membrane-associated receptors, including the family of vacuolar sorting receptors (VSRs). Although many details about the locations and modes of action of VSRs in the trafficking of cargo are currently debated, it is generally agreed that VSRs are essential for the correct trafficking of vacuolar cargo (De Marcos Lousa et al., 2012; Robinson et al., 2012). One model proposed that VSRs bind proproteins at the TGN, release them at the prevacuolar compartments (PVCs), also called multivesicular bodies (MVBs), and return for another round of trafficking (daSilva et al., 2005; Saint-Jean et al., 2010). Vacuolar sorting determinants of cargo act as targeting signals to guide the trafficking of these proteins to the vacuole (Craddock et al., 2008; Miao et al., 2008). Among the vacuolar sorting determinants, the motif NPIR at the N terminus of cargo proteins was proposed to interact with VSRs. Based on in vitro affinity assays, this interaction might be pH dependent (Kirsch et al., 1994; Ahmed et al., 2000) and also Ca²⁺ dependent (Watanabe et al., 2002). These in vitro studies suggested the possible role of pH in regulating receptor and ligand interactions that are necessary for the trafficking of cargo to the vacuole. However, due primarily to the intrinsic limitations of in vitro assays, the specific mechanisms by which pH affects receptor-cargo interactions and how it may alter trafficking to the vacuole have not been addressed. Trafficking mutants, together with in vivo measurements of ion and pH homeostasis, provide indispensable

tools to help our understanding of key processes in the regulation of protein sorting.

Here, we show that two NHX-type antiporters, NHX5 and NHX6, localized to Golgi, TGN, and PVC and are required for storage protein processing and trafficking to storage vacuoles in developing seeds. Using a combination of approaches, including in vivo endomembrane pH measurements, protein-protein interactions, and the biochemical characterization of protein complexes, we provide evidence to suggest that key endomembrane compartments, including those containing VSR and its cargo, require the maintenance of pH homeostasis that is in part regulated by two endosomal antiporters, NHX5 and NHX6. A lack of both antiporters leads to defects in proper protein processing and sorting to storage vacuoles.

RESULTS

Altered Storage Vacuole Morphology and Seed Phenotypes in *nhx5 nhx6* Plants

The *nhx5 nhx6* knockouts displayed striking phenotypes when compared with wild-type plants grown under identical conditions, including large, heavy seeds with a dark coat (Figure 1). On average, *nhx5 nhx6* seeds were 36% larger and nearly 50% heavier than comparable wild-type seeds (Figures 1A to 1D). We previously reported that germination of *nhx5 nhx6* seeds was slightly delayed compared with the wild type but otherwise not inhibited (Bassil et al., 2011a). Given the phenotypes of *nhx5 nhx6* seeds, we examined the morphology of the PSVs of *nhx5 nhx6* seeds. PSVs in seeds exhibit high autofluorescence and therefore have an easily observed morphology. In *nhx5 nhx6* seeds, PSV autofluorescence revealed smaller, less angular PSVs (average diameter of $2.7 \pm 1.1 \mu\text{m}$; $n = 10$) that were more numerous than comparable wild-type PSVs (average diameter of $6.8 \pm 0.9 \mu\text{m}$; $n = 10$) (Figures 1E and 1F). The remarkable difference in size and number of PSVs suggested that aberrant storage vacuole biogenesis or function (i.e., accumulation of storage proteins) might exist in plants lacking functional NHX5 and NHX6 intracellular antiporters.

NHX5 and NHX6 Antiporters Are Required for Storage Protein Processing and Sorting in Developing Seeds

To assess the role(s) of NHX5 and NHX6 in the trafficking and processing of storage proteins, we examined protein profiles of *nhx5 nhx6* seeds and seedlings at different developmental stages. Coomassie blue-stained gels of proteins extracted from maturing, dry seeds and germinated seedlings indicated differences between the *nhx5 nhx6* and wild-type protein profiles at comparable developmental stages (Figure 2A). To confirm the exact nature of these bands, immunoblots probed with anti-2S and anti-12S antibodies, which recognize both mature and unprocessed storage proteins forms (Shimada et al., 2003), were performed on the same protein extracts (Figure 2B). In maturing and dry seeds, bands specific for both p2S (at 17 and 21 kD) and p12S (at 52 kD) were abundant in *nhx5 nhx6* but less so or absent in wild-type immature or dry seeds. These results confirmed the accumulation of unprocessed forms of both storage proteins in the *nhx5 nhx6* knockouts during seed maturation. Interestingly, while p2S accumulated in 3-d *nhx5 nhx6* seedlings,

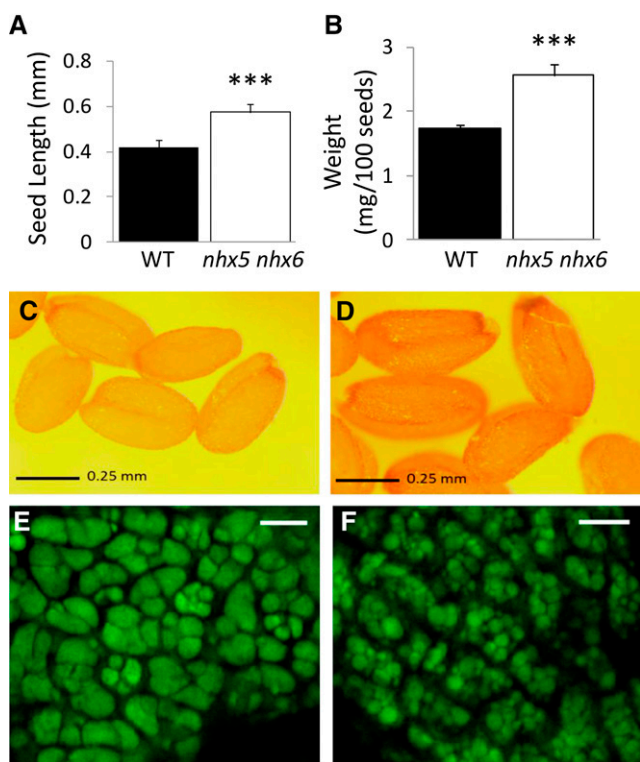


Figure 1. Phenotypes of *nhx5 nhx6* Seed.

Comparison of the size (**A**) and weight (**B**) of wild-type and *nhx5 nhx6* seeds depicted in (**C**) and (**D**), respectively. Autofluorescence of protein storage vacuoles in cotyledons is shown for mature wild-type (**E**) and *nhx5 nhx6* (**F**) seeds. Error bars in (**A**) and (**B**) indicate SD; $n = 300$. Asterisks designate significant differences between genotypes $P \leq 0.001$. Bars in (**C**) and (**D**) = 0.25 mm; bars in (**E**) and (**F**) = 10 μm .

neither processed nor unprocessed storage proteins were detected in 3-d wild-type seedlings or in either 6-d wild-type or *nhx5 nhx6* seedlings. The molecular masses and protein profiles of abnormally accumulated protein forms were similar to those of the precursors of 2S and 12S reported previously (Shimada et al., 2003). Furthermore, the expression of 12S and 2S transcripts was significantly higher in *nhx5 nhx6* dry seeds; 12S transcript levels were also higher in 3-d germinated *nhx5 nhx6* seedlings, whereas 2S transcripts were more abundant in 6-d germinated *nhx5 nhx6* seedlings as compared with the wild type (Supplemental Figure 1). These results would suggest that storage protein synthesis continued in *nhx5 nhx6* after germination and/or that the degradation of mature forms was delayed in knockout 3-d-old seedlings.

During seed maturation and following their processing, 2S and 12S storage proteins accumulate in PSVs (Gruis et al., 2004; Otegui et al., 2006). In order to determine whether the accumulation of storage proteins in the PSV was affected in *nhx5 nhx6*, we examined their subcellular distribution using immunogold labeling in thin sections of dry seeds. In contrast with the wild type, the intercellular spaces of *nhx5 nhx6* embryos were filled with electron-dense material and were notably enlarged (Figure 3; Supplemental Figure 2). The extracellular electron-dense material was recognized by the anti-12S globulin and anti-2S albumin antibodies (Figure 3).

In sections from wild-type embryos, immunolocalization of 12S (Figures 3A and 3B) and 2S (Figures 3C and 3D) storage proteins was exclusive to the PSVs, whereas in *nhx5 nhx6*, relatively few gold particles of both anti-12S and anti-2S were found within PSVs compared with those in the apoplast (Figures 3E to 3H). For example, the density of gold particles in wild-type PSVs was 2-fold higher than in *nhx5 nhx6* PSVs (88 ± 7 versus 40 ± 4 gold particles/ μm^2 ; $n = 12$), while the density of those in the apoplast was 15-fold higher in the knockout (132 ± 13 versus 8 ± 1 gold particles/ μm^2 ; $n = 12$). These results suggested that storage proteins were missorted to the apoplast in *nhx5 nhx6*, possibly causing the enlargement of the extracellular space and the reduction of PSV sizes.

Since the anti-2S and anti-12S antibodies that were used in immunogold localizations (Figure 3) did not distinguish between unprocessed and processed storage protein forms, we performed additional immunogold labeling of embryo thin sections using an antibody that specifically recognizes unprocessed 2S albumin forms (Otegui et al., 2006). In the same dry seed sections, we found that unprocessed 2S albumins were also abundant in the *nhx5 nhx6* extracellular space (Figures 3I to 3L), suggesting that the missorting of 2S occurs at a step prior to their reaching MVBs,

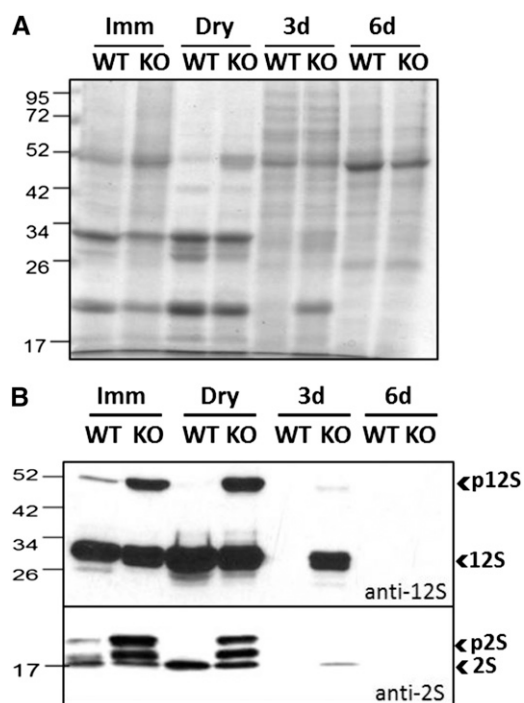


Figure 2. Storage Protein Profile in Maturing, Dry, and Germinating *nhx5 nhx6* Seeds.

(A) Seed protein profile (Coomassie blue-stained gel) collected at different developmental stages: immature (Imm), dry, and either 3 or 6 d after germination. The wild type (WT) and *nhx5 nhx6* (KO) were loaded in alternate lanes.

(B) Immunoblot of protein extracts (from **[A]**) probed using anti-12S and anti-2S antibodies. In *nhx5 nhx6* (F37), an accumulation of pro forms (immature) of both 12S (top blot) and 2S (bottom blot) storage proteins is evident. Mature forms (2S and 12S) persisted in *nhx5 nhx6* seeds 3 d after germination.

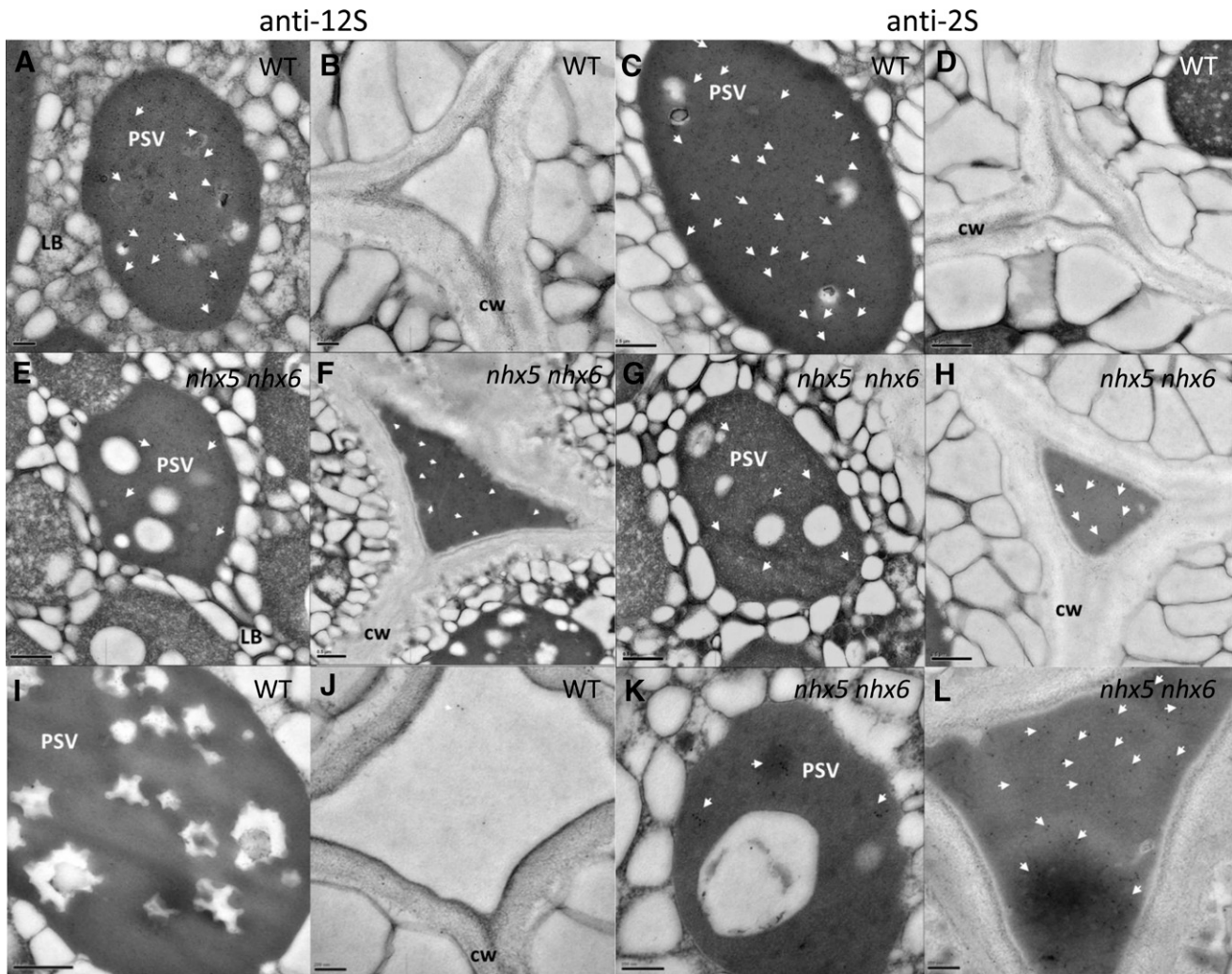


Figure 3. Subcellular Localization of Storage Proteins in Seeds Requires NHX5 and NHX6.

Transmission electron micrographs of dry wild-type seeds (**[A]** to **[D]**) indicate the accumulation of electron-dense material in the extracellular space of *nhx5 nhx6* (**[E]** to **[H]**). Immunogold labeling (10-nm gold particle) localized 12S globulin (**[A]**, **[B]**, **[E]**, and **[F]**) and 2S albumin (**[C]**, **[D]**, **[G]**, and **[H]**) in the apoplast of *nhx5 nhx6* mature seeds. Immunolocalization of the pro form of 2S albumin in dry seeds using anti-N-terminal 2S antibody followed by immunogold labeling (10-nm gold particle) recognized the precursors of 2S albumin (immature/unprocessed) (**[I]** to **[L]**). Wild-type seed sections of storage vacuole (**[I]**) and middle lamella (**[J]**) and *nhx5 nhx6* seed sections of storage vacuole (**[K]**) and middle lamella (**[L]**) are shown. CW, cell wall; LB, lipid body. Quantification of the number of immunogold particles in the apoplast and storage vacuole is presented in Results. White arrowheads point to gold particles. Bars in (**A**) and (**B**) = 0.2 μm ; bars in (**C**) to (**I**) = 0.5 μm ; bars in (**J**) to (**L**) = 200 nm.

where proteolytic processing is thought to occur (Otegui et al., 2006). The presence of some immature 2S proteins inside the vacuoles might indicate that incomplete processing occurred in *nhx5 nhx6* seeds.

In order to assess whether the ER was affected in *nhx5 nhx6*, we quantified the expression of the unfolded protein response (UPR) genes as a measure of ER stress. No differences in the expression of these UPR genes were found between *nhx5 nhx6* and wild-type seeds and seedlings (Supplemental Figure 3).

To determine structural alterations in the endomembrane system that could account for the missorting of storage protein precursors to the apoplast, we analyzed high-pressure frozen, freeze-substituted embryos by immunogold labeling. As reported

previously, the antibodies that recognize the 2S large subunit, the N-terminal propeptide in 2S precursors, and VSR were localized to the Golgi, Golgi-derived compartments, and MVBs in both wild-type and *nhx5 nhx6* embryos (Figures 4A to 4J) (Otegui et al., 2006). However, we found an unusual accumulation of vesicle clusters containing precursors of 2S albumins and VSR in the *nhx5 nhx6* embryos (Figures 4B, 4E, 4F, 4H, and 4J). We estimated the possible missorting of VSR to the plasma membrane of *nhx5 nhx6* seed embryo cells using anti-VSR immunogold localization. A quantification of the distribution of anti-VSR gold particles indicated that, in *nhx5 nhx6* embryo cells, a significantly higher density of VSR was found at the plasma membrane than in comparable wild-type cells (Supplemental Figure 4). These results suggest that

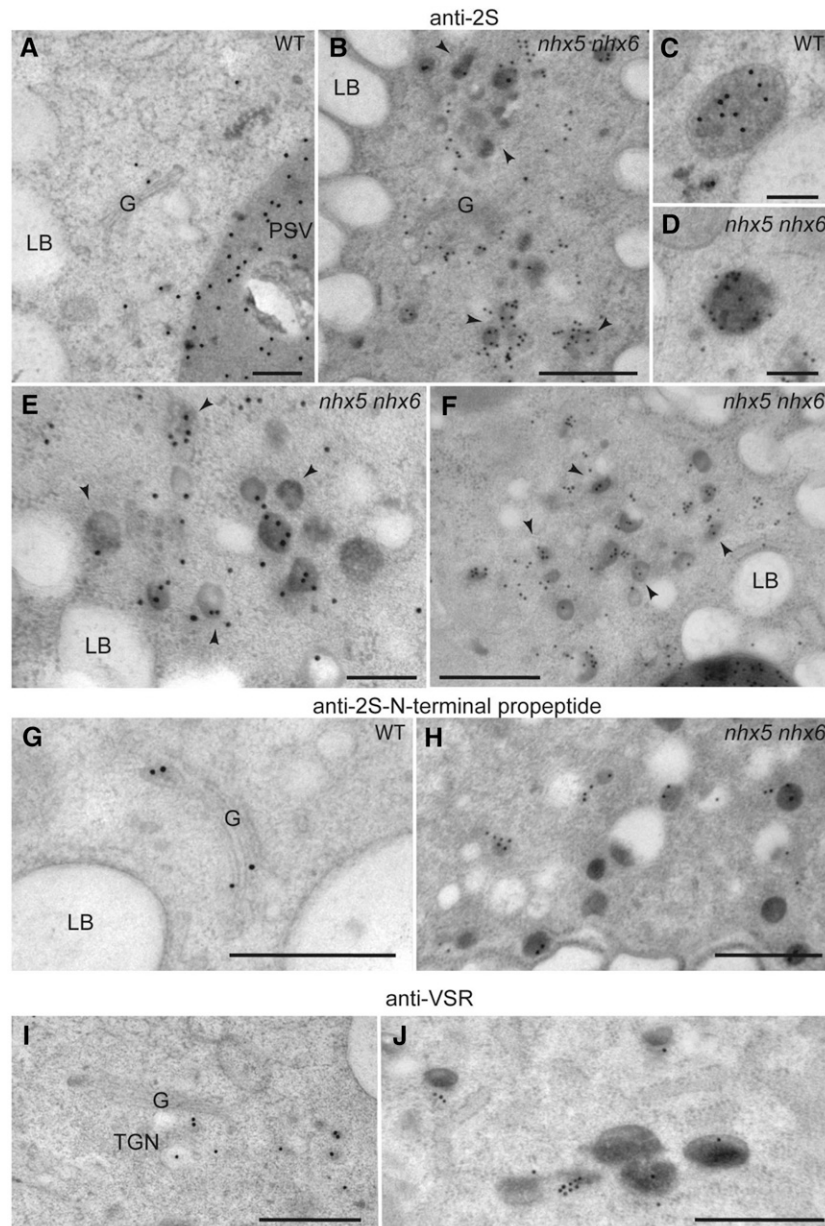


Figure 4. Immunogold Labeling of High-Pressure Frozen, Freeze-Substituted Embryos.

(A) to (F) Wild-type (A) and (C) and *nhx5 nhx6* mutant (B), (D), (E), and (F) embryo cells labeled with antibodies against the 2S large subunit. (C) and (D) show MVB/PVC-containing storage proteins. Notice the accumulation of large clusters of vesicles containing 2S albumins in *nhx5 nhx6* cells (B), (E), and (F), arrowheads).

(G) and (H) Wild-type (G) and *nhx5 nhx6* mutant (H) embryo cells labeled with antibodies against the 2S N-terminal propeptide.

(I) and (J) Wild-type (I) and *nhx5 nhx6* mutant (J) embryos labeled with anti-VSR antibodies.

G, Golgi; LB, lipid body. Bars in (A), (C), and (D) = 200 nm; bars in (B) and (E) to (J) = 500 nm.

vesicle clusters carrying the storage protein precursors to the apoplast fuse with the plasma membrane.

NHX5 Colocalizes to the TGN and PVC

Previously, we assessed the localization of NHX5 and NHX6 using immunogold localization and colocalization with subcellular markers

and found high colocalization between NHX5 and NHX6 at the Golgi and TGN (Bassil et al., 2011a). Here, we performed additional colocalization studies using alternate markers for the TGN and for well-known markers of the PVC in order to better characterize the distribution of NHX5 in the endomembrane system. We crossed plants expressing NHX5-YFP (for yellow fluorescent protein) with stable reporters of VT112-RFP (for red fluorescent protein), ARA7-RFP,

and Rha1-RFP (Geldner et al., 2009) and assessed the extent of colocalization in mature zone root cells as described in Methods. Using two statistical measures of colocalization (Li's ICQ and Pearson's correlation coefficient [PSC]), we found that NHX5 was highly colocalized with the TGN SNARE, VTI12 (Figures 5A to 5C; PSC = 0.80 ± 0.1 ; ICQ = 0.32 ± 0.07), and showed less colocalization with the PVC markers ARA7 (Figures 5E to 5G; PSC = 0.65 ± 0.05 ; ICQ = 0.28 ± 0.03) and Rha1 (Figures 5I to 5K; PSC = 0.62 ± 0.1 ; ICQ = 0.27 ± 0.013). These data indicated that NHX5 was predominantly distributed in the TGN but also existed in the PVC, suggesting that it may traffic between the two compartments.

The Luminal pH of TGN, PVC, and VSR Compartments Is More Acidic in the *nhx5 nhx6* Mutant

Given the proposed biochemical function of NHX5 and NHX6 in H^+ transport, we sought to measure the luminal pH of different endomembrane compartments in *nhx5 nhx6*. We used a set of ratiometric, genetically encoded pHluorin-based pH sensors in a translational fusion with VSR2;1 (pH-VSR2;1) in which pHluorin was placed in the luminal domain of VSR2;1. This sensor was used previously to measure the luminal pH of VSR compartments in the TGN and PVC (Martinière et al., 2013). Expression of these pH sensors resulted in pH-dependent fluorescence ratios that can be used to calculate the luminal pH of VSR vesicles in live protoplasts (Figure 6). To relate pHluorin fluorescence ratios to pH, we performed an in vivo calibration using nigericin and high K^+ (Kim et al., 1996; Kneen et al., 1998) over the range of pH values indicated in Figure 6A. We reasoned that in vivo calibration would result in pH ratios that better reflect the endogenous vesicle environment. The ratio values obtained over the pH range 6 to 7 allowed for robust measurements of luminal pH. We assessed whether the pH in either the Golgi, TGN, or PVC was different in *nhx5 nhx6* using the previously characterized pH probes ST-pH, pH-VSR-Y, and pH-VSR-IM, which localize specifically to the Golgi, TGN, and late PVC, respectively (Martinière et al., 2013). Representative rainbow-colored images of the ratio of fluorescence of representative wild-type and *nhx5 nhx6* protoplasts expressing pH-VSR2;1 are shown in Figures 6B and 6C, respectively, and indicated that the average pixel intensities of VSR compartments in the wild type were higher (white-red color in the center of compartments) than those of *nhx5 nhx6*. pH measurements obtained using these probes revealed that the TGN in the wild type (pH 6.25) was significantly more acidic than that of the late PVC (pH 6.9) and the Golgi (pH 6.7) (Figure 6D). This trend was similar in *nhx5 nhx6* protoplasts; however, the pH of the Golgi, TGN, and late PVC was significantly more acidic in *nhx5 nhx6* than in the wild type. The pH was most aberrantly acidic in *nhx5 nhx6* late PVC (Δ pH of 0.4), compared with Δ pH of 0.25 in the TGN and Golgi. pH values are consistent with NHX5 localization and suggest that NHX5 and NHX6 contribute to the pH homeostasis of the Golgi, TGN, and PVC.

Given the possible importance of pH for the interaction between VSR and its cargo aleurain (Ahmed et al., 2000), we wanted to measure directly the luminal pH of VSR-positive compartments that contain the VSR cargo aleurain. We coexpressed pH-VSR2;1 and aleurain and measured the pH in colocalized vesicles. We found that the luminal pH of VSR2;1 *nhx5 nhx6* compartments containing aleurain was significantly more acidic (pH 6.10 ± 0.12 , $n > 150$

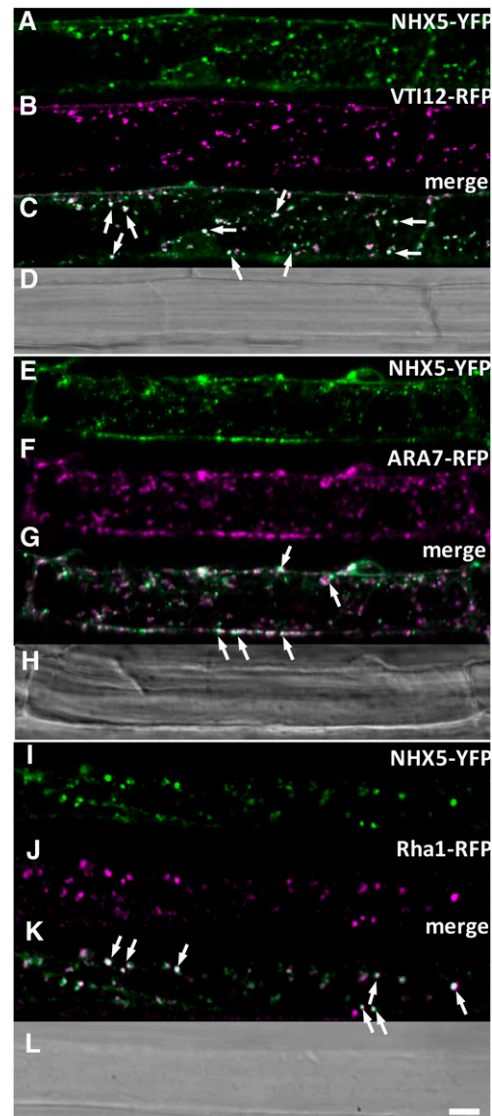


Figure 5. Colocalization of NHX5 with Subcellular Markers of the TGN and PVC.

(A) to (D) NHX5-YFP and VTI12-RFP.

(E) to (H) NHX5-YFP and Ara7-RFP.

(I) to (L) NHX5-YFP and Rha1-RFP.

Single-channel images of NHX5-YFP are shown in (A), (E), and (I), those of VTI12-RFP are shown in (B), those of ARA7-RFP are shown in (F), and those of Rha1-RFP are shown in (J). Merged images of NHX5-YFP and the corresponding marker are shown in (C), (G), and (K). Colocalization was assessed in the F1 cross of stable expressing parents. Representative images are taken from the mature zone of root cells in 3-d-old seedlings. Bar = 10 μ m.

vesicles from at least 20 protoplasts) than comparable wild-type VSR-aleurain compartments (pH 6.70 ± 0.09 ; $n > 150$ vesicles from at least 20 protoplasts) (Figure 6E). The difference of 0.6 pH units is highly statistically significant ($P \leq 0.001$). The aberrant luminal pH in *nhx5 nhx6* VSR-aleurain vesicles, therefore, could affect the VSR-aleurain interaction in *nhx5 nhx6* cells.

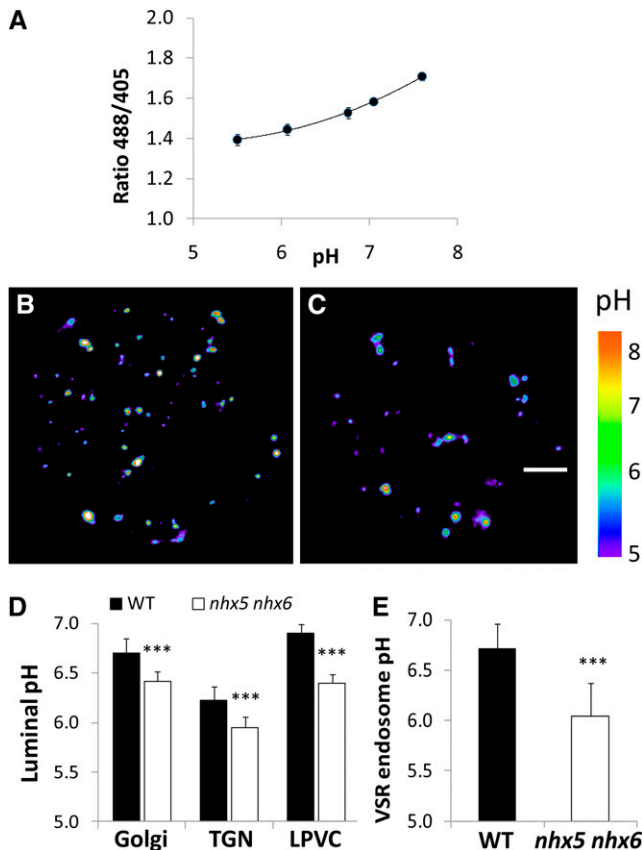


Figure 6. In Vivo pH of Intracellular Compartments in *nhx5 nhx6* Cells.

(A) In vivo calibration curve of endosomal pH. pH calibration was achieved by equilibrating intracellular pH with 10 μ M nigericin, 60 mM KCl, and 10 mM MES/HEPES Bis-Tris-propane, pH 5.5 to 7.5.

(B) and **(C)** Pseudocolored images of the fluorescence ratio (emission 500 to 550 nm from excitation with 488 nm/emission 500 to 550 nm from excitation with 405 nm) resulting from VSR2;1-pHluorin expression in a representative wild-type **(B)** or *nhx5 nhx6* **(C)** protoplast. The rainbow scale correlates to pH. Bar = 5 μ m.

(D) Luminal pH of Golgi, TGN, and the late prevacuolar compartment (LPVC) measured using the compartment-specific pH probes described in Methods. *** $P \leq 0.001$; $n > 150$ from at least 20 protoplasts.

(E) Endosomal pH in protoplasts transiently expressing VSR2;1-pHluorin and Aleu-mRFP indicates that the luminal pH of VSR endosomes that colocalize with aleurain are more acidic in *nhx5 nhx6* cells. *** $P < 0.001$, by *t* test.

VSR Receptor Cargo Interactions Are Compromised in the *nhx5 nhx6* Knockout

The requirement of VSR for the proper trafficking of storage proteins such as 12S and 2S to PSVs is known (Shimada et al., 2003; De Marcos Lousa et al., 2012), and the missorting of unprocessed storage proteins in *nhx5 nhx6* (Figure 3) would suggest that the binding of storage protein cargo with VSR might be affected. We examined the abundance of VSR1;1 as well as VSR1;1 gene expression in seeds and seedlings of the wild type and *nhx5 nhx6* knockouts. Similar amounts of VSR1;1 between the wild type and *nhx5 nhx6* were detected at the immature seed stage, but VSR1;1 accumulated in *nhx5 nhx6* at the end of seed development

(Supplemental Figure 5). The appearance of two or more bands of different molecular masses in both the wild type and *nhx5 nhx6* might be due to different glycosylated forms of VSRs (De Marcos Lousa et al., 2012) or different VSR isoforms recognized by VSR1;1 antibody. Given the accumulation of VSR1;1 in *nhx5 nhx6*, its importance in the sorting of cargo to storage vacuoles (Shimada et al., 2003), and the similarities between *nhx5 nhx6* and *vsr1* phenotypes, we sought to investigate whether the association of the VSR1;1 receptor with its cargo might be altered in *nhx5 nhx6* and whether this was associated with incomplete storage protein processing and missorting. Putative protein complexes of VSR and its cargo were isolated from immature seeds under nonreducing conditions and resolved using 2D blue-native PAGE (BN-PAGE)/SDS-PAGE followed by immunoblotting. Intact complexes were run according to size in the first dimension (approximately at 480 kD for putative p12-VSR complex, considering VSR dimerization [Kim et al., 2010] and the formation of p12S hexamers of 54-kD subunits [Fujiwara et al., 2002]) and subsequently separated into their individual components when run in the second dimension (i.e., denaturing conditions) (VSR at 80 kD, p12S at 52 kD, and 12S at 34 kD). Components of a particular complex will occur as spots vertically above/below each other in the final blots (Wittig et al., 2006). 2D BN-PAGE of immature seed protein extracts indicated that in *nhx5 nhx6*, the intensities of several spots corresponding to protein complexes differed significantly from those of the wild type (Figure 7; Supplemental Figures 6D and 6E). We identified VSR1;1, and p12S in complexes by successively immunolabeling the same blot (after stripping) with the antibodies α -VSR (Yamada et al., 2005) and α -12S (Shimada et al., 2003). Immunoblots revealed that VSR complexes in the first dimension occurred in sizes between 480 and 242 kD, probably representing VSR complexes with different cargo (Figure 7). The occurrence of an additional lower molecular mass VSR spot (i.e., lower than 80 kD in the second dimension) might indicate the presence of other VSR isoforms. The amount of VSR1;1 (top blots) was not significantly different between *nhx5 nhx6* and the wild type (Supplemental Figure 7B). In the wild type, p12S signal appeared at a higher molecular mass than 480 kD in the first dimension (bottom left blot in Figure 7) (Hara-Nishimura et al., 1998) and was significantly reduced in *nhx5 nhx6*. The VSR signal associated with p12S appeared, as expected, in the same vertical line at 480 kD in the first dimension (Figure 7), shown after superposing blot images of the same membrane. The quantification of the relative signals of VSR and p12S (see BN-PAGE section in Methods and Supplemental Figure 6) in wild-type and *nhx5 nhx6* complexes indicated that the overall p12S signal associated with VSR was reduced significantly (approximately three times) in *nhx5 nhx6* as compared with the wild type (Figure 6). Given the higher amounts of p12S found in *nhx5 nhx6* (Figure 2), the reduction in the p12S signal associated with VSR (Figure 6) was not likely due to a decrease in the amount of p12S but rather to a reduction in the interaction between p12S and the VSR. These results suggest that receptor-cargo interaction might be compromised in plants lacking NHX5 and NHX6 antiporters.

To investigate further VSR-mediated trafficking to the vacuole, and to test the direct in vivo interaction between VSR and another cargo protein (aleurain), we used bimolecular fluorescence complementation (BiFC) and live cell imaging. BiFC is based on the association of two fluorescent protein halves that result in

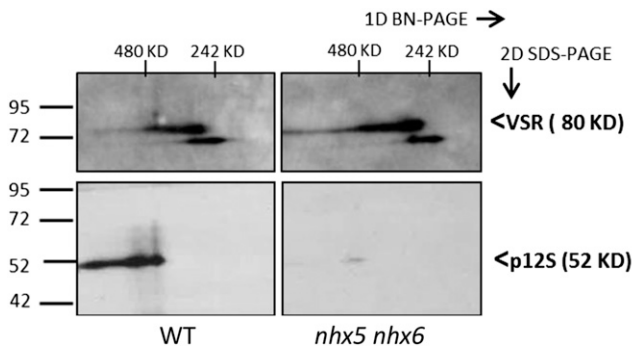


Figure 7. Separation and Identification of VSR Receptor-Aleurain Cargo Complexes Using 2D BN-PAGE/SDS-PAGE.

Native complexes were separated using 2D BN-PAGE/SDS-PAGE (4 to 16% acrylamide gradient gel) in the first dimension (left to right) followed by SDS (10% acrylamide) in the second dimension (top to bottom) in the wild type (left) and *nhx5 nhx6* (right). Forty-five micrograms of total protein from immature seed tissue was loaded on each gel. Immunoblots of anti-VSR1;1 (top) and anti-p12S (bottom) are indicated. Signals were quantified from scanned images as described in Methods using four different repetitions of the experiment (one representative set of blots is shown). Wild-type complexes had 3.0 ± 0.9 times more p12S associated with VSR compared with *nhx5 nhx6*. For each antibody, the same blot exposition time and scan settings were used for the wild type and *nhx5 nhx6*.

a complementation of a fluorescent complex when the halves are brought together by an interaction between the targeted proteins fused to these halves (Hu et al., 2002). Aleu-VYNE, aleurain fused to the N-terminal half of Venus, and SCYCE-VSR2;1, expressing the C-terminal half of super cyan fluorescent protein fused to the N terminus of VSR2;1 (between the signal peptide and the luminal domain), were coexpressed in isolated leaf mesophyll protoplasts (Figure 8). We used VSR2;1 (VSR4) because this isoform was used previously as a pH sensor to measure the luminal pH of VSR2;1-positive compartments (Martinière et al., 2013). We looked for the presence of a 515-nm (green) emission signal, resulting from BiFC, as an indication of interaction between VSR2;1 and aleurain. A positive transformation control, expressing a VSR1-mRFP that properly localized but did not competitively bind to its cargo (Park et al., 2007) and therefore would not compete with SCYCE-VSR2;1, was cotransformed with the BiFC plasmids in order to assess the colocalization of any BiFC signal (Figure 8B). This “inactivated” VSR1-mRFP also served as an internal control to normalize signals needed to quantify any VSR-aleurain interaction (discussed below). As shown in Figure 8, cotransformation of SCYCE-VSR2;1 and Aleu-VYNE in wild-type protoplasts resulted in the appearance of green fluorescent punctae that were consistent with the VSR expression patterns, strongly suggesting that an *in vivo* interaction between VSR2;1 and aleurain had occurred. Furthermore, the green fluorescence resulting from BiFC colocalized highly with VSR1-mRFP-labeled compartments (PSC = 0.86 ± 0.15 , ICQ = 0.42 ± 0.08 in wild-type protoplasts and PSC = 0.83 ± 0.12 , ICQ = 0.40 ± 0.08 in *nhx5 nhx6* protoplasts). In *nhx5 nhx6* protoplasts, fluorescence complementation also resulted in green punctae that colocalized with VSR1-mRFP, but their number was significantly reduced (Figures 8E and 8G) compared with the wild type (Figure 8C). The number of VSR1-mRFP vesicles

was not significantly different between *nhx5 nhx6* and wild-type protoplasts (Figures 8B and 8F; Supplemental Figure 8). Because protoplasts were handled and imaged identically, we approximated the extent of the VSR-aleurain interaction by comparing the number of green fluorescent compartments as well as their relative fluorescence intensities (see Methods). A comparison of green and red fluorescence ratios, instead of absolute green fluorescence intensity, provided a measure of the relative difference in the VSR-aleurain interaction that would be independent of differences in transformation efficiency and/or expression. As shown in Figure 8, not only was the number of BiFC bodies significantly reduced in *nhx5 nhx6* protoplasts (Figure 8I) but also the relative fluorescence intensity within each body was reduced (Figure 8J). We also examined whether the interaction of VSR2;1 with another cargo, p12S, might be similarly affected in *nhx5 nhx6*. Cotransformation of SCYCE-VSR2;1 with p12S-VYNE produced similar results, with marked reduction of BiFC in *nhx5 nhx6* protoplasts, to those seen in experiments using SCYCE-VSR2;1 and Aleu-VYNE (Supplemental Figure 8). These data suggested that the receptor-cargo interaction is generally affected in *nhx5 nhx6* and not unique to the interaction of VSR with aleurain.

It is possible that differences in the expression of interacting partner proteins caused the reduced BiFC seen in *nhx5 nhx6*; therefore, we estimated the abundance of partner proteins in extracts from protoplasts expressing SCYCE-VSR2;1 with p12S-VYNE (Supplemental Figure 9). Immunoblots probed using α -GFP indicated that similar amounts of both interacting partners (SCYCE-VSR2;1 [110 kD] and p12S-VYNE [80 kD]) were present in both wild-type and *nhx5 nhx6* BiFC-expressing protoplasts (Supplemental Figure 9), confirming that the reduction in BiFC signal seen in *nhx5 nhx6* was not due to a lower abundance of BiFC partner proteins in protoplasts.

To assess potential consequences of the BiFC interaction to trafficking or localization, we assessed and compared the subcellular localization of either BiFC vesicles or VSR2;1 in wild-type and *nhx5 nhx6* protoplasts (Supplemental Figure 10). As markers, we used soybean (*Glycine max*) Man1 for the Golgi (Saint-Jore-Dupas et al., 2006), Syp61 for the TGN (Foresti and Denecke, 2008), and ARA7 for the PVC (Nielsen et al., 2008). The results indicated that BiFC bodies colocalized highly with ARA7 (PSC = 0.82) and only poorly with Man1 (PSC = 0.44), while colocalization with Syp61 was intermediate (PSC = 0.69) (Supplemental Figure 10A). Importantly, this distribution was not different between the wild type and *nhx5 nhx6*. Similarly, the colocalization of VSR2;1 was also highest with ARA7 (PSC = 0.83) and least with Man1 (PSC = 0.41) and was not different between the wild type and *nhx5 nhx6*. Because the respective PSC values between BiFC bodies or VSR2;1 and the subcellular markers were not significantly different between the wild type and *nhx5 nhx6*, we conclude that BiFC probably did not alter trafficking significantly.

In Vivo Interaction between VSR and Aleurain Is pH Dependent

Given both the abnormally acidic pH of *nhx5 nhx6* VSR-positive compartments and the reduced interaction between VSR and aleurain, we examined the role of intravesicular pH in VSR-aleurain binding. Using BiFC, we assessed VSR-aleurain interactions (as described in Figure 8), but instead, we equilibrated the pH across

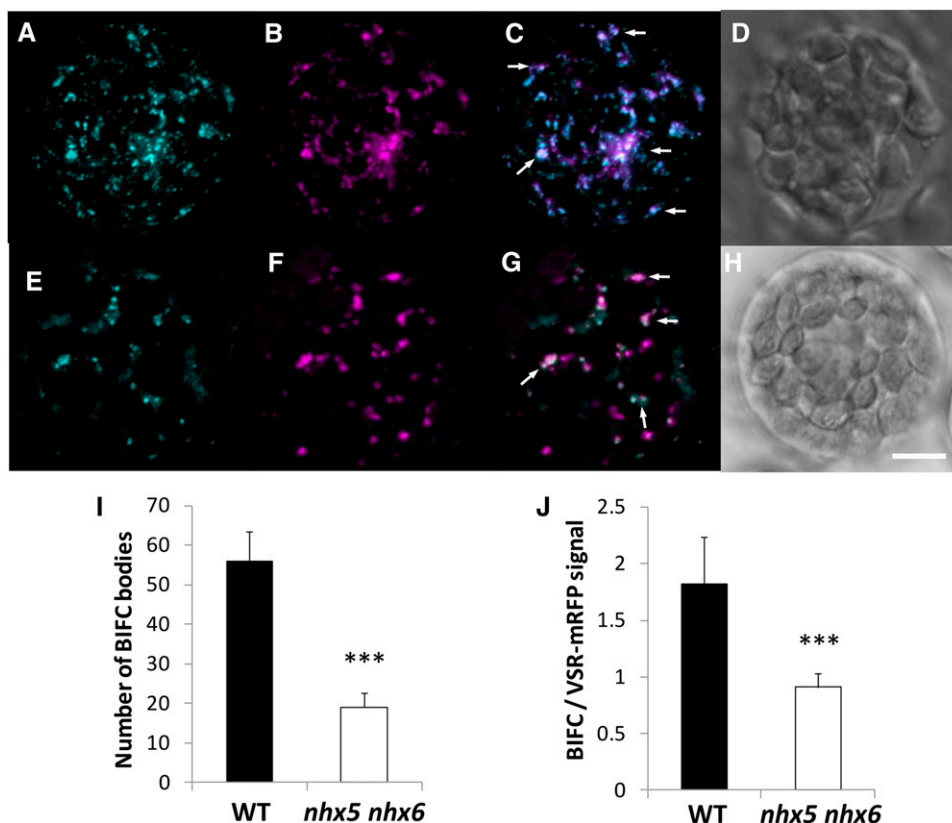


Figure 8. In Vivo Interaction between the VSR Receptor and Its Cargo Protein Aleurain.

Interaction is visualized as BiFC between aleurain fused at the C terminus to the N-terminal half of Venus (Aeu-VYNE) with the C-terminal half of super cyan fluorescent protein (SCYCE) fused to the N terminus of VSR2;1 (SCYCE-VSR2;1) in isolated mesophyll protoplasts. Images are 3D projections of a series of four to five z-stack images and shown in the wild type (**A**) and *nhx5 nhx6* (**E**). An inactivated VSR1;1-mRFP that properly localizes to VSR-positive compartments was used as a transformation control in the wild type (**B**) and *nhx5 nhx6* (**F**) (see Methods). (**C**) shows merged images of (**A**) and (**B**) in the wild type, and (**G**) shows merged images of (**E**) and (**F**) in *nhx5 nhx6*. Differential interference contrast images of the wild type and *nhx5 nhx6* are shown in (**D**) and (**H**), respectively. (**I**) and (**J**) show quantification of the number of BiFC bodies (**I**) and the BiFC signal intensity relative to the VSR1;1-mRFP control (**J**). Error bars indicate sd; $n = 75$. *** $P < 0.001$, by t test. Bar = 5 μm .

intracellular compartments. We reasoned that if the acidic pH of VSR compartments in *nhx5 nhx6* was responsible for the reduced interaction between VSR and aleurain, then alkalization of VSR compartments might partially rescue this reduced interaction in the *nhx5 nhx6* mutants. We incubated wild-type protoplasts from Figure 8 that were already exhibiting SCYCE-VSR2;1 and Aleu-VYNE fluorescence complementation and equilibrated the intracellular pH with a buffer at pH 5.0 (using nigericin and high K^+ , as was done for pH calibration in Figure 6). When compared with unequilibrated protoplasts (Figure 8A), acidified wild-type protoplasts did not differ in the number of BiFC bodies or their signal intensity or in the number and intensity of VSR1-mRFP vesicles (Figures 9A and 9E). The BiFC signal remained constant for up to 30 min, after which protoplasts began to display visible deterioration. In a different experiment, *nhx5 nhx6* protoplasts exhibiting SCYCE-VSR2;1 and Aleu-VYNE fluorescence complementation (as shown in Figure 8G) were alkalized with pH 7.0 buffer (i.e., intracellular pH was equilibrated to pH 7.0 with nigericin and high K^+ , as was done for pH calibration in Figure 6A). A quantification of BiFC indicated that the number of BiFC bodies not only doubled (Figure 9E) but that their

relative fluorescence intensity, compared with the VSR1-mRFP control, increased by 60% (Figure 9F), suggesting that an acidic pH in *nhx5 nhx6* VSR/aleurain vesicles likely caused the reduced interaction observed in the BiFC assay.

To test whether the reduced BiFC signal was due to fluorescence quenching at acidic pH rather than a bona fide decrease in VSR-aleurain interaction, we generated a chimeric protein between SCYCE and VYNE ("chimera") and tested its fluorescence response when expressed in protoplasts whose intracellular pH was equilibrated with acidic buffers. To create this chimeric protein, we used as a template the constructs described by Gehl et al. (2009) to make 35S:VYNE-SCYCE, which expressed VYNE fused to SCYCE (see Methods). Transformation of this chimera in wild-type protoplasts resulted in strong cytosolic green fluorescence emission, as indicated in the 3D reconstructed z-stack image (Figure 10). We quantified fluorescence before and after the acidification of intracellular pH, achieved by equilibrating the internal pH with external acidic pH using nigericin and high K^+ , as was done previously. The fluorescence intensity of the SCYCE-VYNE chimeric protein in acidified protoplasts did not differ appreciably from the fluorescence

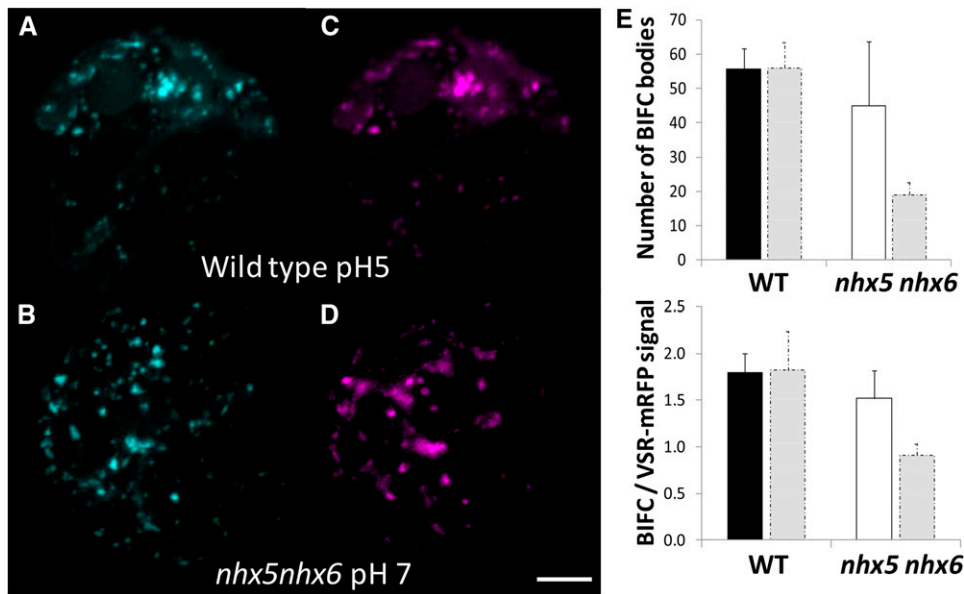


Figure 9. Intracellular Alkalinization Improves the in Vivo Interaction of VSR with Aleurain in *nhx5 nhx6*.

(A) BiFC in wild-type protoplasts coexpressing SCYCE-VSR2;1 and Aleu-VYNE and equilibrated with acidic buffer, pH 5. A comparison of the resulting signal, expressed as both number of BiFC bodies and BiFC signal relative to the transformation control (VSR1;1-mRFPm) signal, as was done in Figure 8, is shown in (E) and (F) below.

(B) BiFC in *nhx5 nhx6* protoplasts coexpressing SCYCE-VSR2;1 and Aleu-VYNE and incubated in alkaline equilibration buffer, pH 7. pH was equilibrated in both the wild type and *nhx5 nhx6* with 10 μ M nigericin, 60 mM KCl, and 10 mM MES/Bis-Tris-propane, pH 5.0 or 7, similar to the in vivo pH calibration described in Methods and Figure 7.

(C) and (D) Expression of inactivated VSR1;1-mRFP control in the wild-type (C) and *nhx5 nhx6* (D) protoplasts shown in (A) and (B), respectively. Bar = 5 μ m.

(E) and (F) Quantification of the number of BiFC bodies (E) and quantification of the BiFC signal relative to inactivated VSR1;1-mRFP (F), shown in (A) and (B). Bars are means of 65 protoplasts \pm SD. Gray bars indicate control values from unequilibrated wild-type and *nhx5 nhx6* protoplasts in Figure 8 and are included for comparison with the equilibrated protoplasts presented here. Protoplasts were incubated with pH buffers for 15 min before imaging. Error bars indicate SD. *** $P < 0.001$, ** $P < 0.01$, by t test.

of unequilibrated protoplasts (relative fluorescence value of 0.97; Figure 10A). As a control, we also quantified the pH-dependent fluorescence of PIP2;1-GFP-expressing protoplasts. PIP2;1-GFP localizes to the plasma membrane with the GFP moiety facing the cytosol, as determined by several topology prediction programs (http://aramemnon.botanik.uni-koeln.de/tm_sub.ep?GeneID=11767&ModelID=0). Unlike the chimeric SCYCE-VYNE protein, the acidification of PIP2;1-GFP-expressing protoplasts (Figure 10C) resulted in a marked reduction in PIP2;1-GFP relative fluorescence, because acidified protoplasts had 30% of the fluorescence intensity of unequilibrated protoplasts (Figure 10A). These results suggested that the reconstituted SCYCE-VYNE resulted in green fluorescence emission that did not quench at acidic pH, as occurred with GFP.

VSR Receptor and Cargo Do Not Significantly Mislocalize in *nhx5 nhx6*

One possible cause for the reduced interaction between VSR2;1 and aleurain in *nhx5 nhx6* protoplasts could be the mislocalization of aleurain and/or VSR2;1. To assess the degree of aleurain colocalization with VSR2;1 in vivo, we coexpressed VSR2;1-GFP and Aleu-mRFP in isolated protoplasts (Figure 11). In merged images of the wild type (Figure 11C) and *nhx5 nhx6* (Figure 11G), we observed

a large number of compartments labeled with both fluorescent proteins, indicating a high degree of colocalization between VSR2;1-GFP and Aleu-mRFP in both the wild type and *nhx5 nhx6* (arrows). We quantified colocalization in two ways: (1) the overlap of the total VSR2;1-GFP and Aleu-mRFP signals in each protoplast; and (2) the colocalization of Aleu-mRFP in VSR2;1-GFP vesicles. In the former, we estimated a lower PSC between VSR2;1 and aleurain in *nhx5 nhx6* compared with the wild type ($P \leq 0.05$; Figure 11I). In the second analysis, in which we asked how much aleurain colocalized with VSR vesicles specifically, the PSC coefficient between VSR2;1-GFP and Aleu-mRFP was not significantly different between the wild type and *nhx5 nhx6* (Figure 11J). Collectively, these data support the notion that, although a small fraction of the aleurain signal was distinctly localized from VSR2;1 in *nhx5 nhx6*, a significant proportion of aleurain remained colocalized with VSR2;1 vesicles.

DISCUSSION

pH in the Endomembrane System

The tight regulation of intracellular pH is essential to myriad biological processes in all organisms. Changes to cellular pH homeostasis, which are achieved by the action of both H^+ pumps and leaks, occur

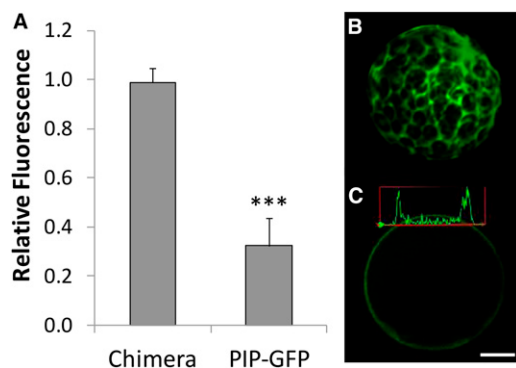


Figure 10. Quantitative Comparison of pH-Dependent Fluorescence in Protoplasts.

The fluorescence (emission 500 to 550 nm) of two proteins was compared at acidic intracellular pH relative to control protoplasts (i.e., whose intracellular pH was not equilibrated) (**A**). Intracellular and extracellular pH was equilibrated with 10 μ M nigericin, 60 mM KCl, and 10 mM MES-Bis-Tris-propane, pH 5, similar to the *in vivo* calibration (see Methods and Figure 7). Error bars indicate sd. *** $P < 0.001$, by *t* test. In Chimera, protoplasts were transformed with the construct VYNE-SCYCE, which resulted in green fluorescence emission in the cytosol (shown in **B**) as a 3D reconstruction of seven z-stack slices). (**C**) shows the transient expression of PIP1;2-GFP quantified in (**A**) and localized at the plasma membrane. A fluorescence intensity plot across a line that transects the protoplast at two points is shown, which was used to calculate relative fluorescence. Bar = 5 μ m.

throughout development and in response to diverse environmental cues (Casey et al., 2010). Pumps include the plasma membrane P-type H⁺-ATPase, V-ATPase, and H⁺-pyrophosphatase, while H⁺ efflux from the lumen of intracellular compartments is provided by cation exchangers including the NHX type. In animals, intracellular pH is fine-tuned to specific values in different endomembrane compartments (Paroutis et al., 2004) and is similar to what has been reported recently in plants (Martinière et al., 2013; Shen et al., 2013). Pharmacological and genetic evidence have suggested that maintaining acidic TGN is critical for cellular trafficking, cell expansion, and cell wall composition (Dettmer et al., 2006; Brück et al., 2008). For example, concanamycin A and bafilomycin A, two inhibitors of V-ATPases, caused the secretion of soluble vacuole-targeted proteins and the blocking of secreted proteins and the endocytosis tracer FM4-64 (Matsuoka et al., 1997; Dettmer et al., 2006; Brück et al., 2008). The localization at the TGN of the α 1 subunit of the V-ATPase complex, along with evidence from functional knockouts, also implicate this H⁺ V-ATPase in protein trafficking (Dettmer et al., 2006; Brück et al., 2008). Luminal acidification alone is not sufficient to maintain pH homeostasis, as suggested by studies in animals and yeast that firmly demonstrated the importance of NHX-type antiporters for pH regulation and protein trafficking (Orlowski and Grinstein, 2011). In yeast, protein trafficking out of the Golgi was blocked in *Nhx1* Δ (Bowers et al., 2000), and the mutant had altered cytosolic and vacuolar pH (Brett et al., 2005). Direct evidence for a role of NHX in vesicular trafficking in plants was initially provided by the double knockout lacking NHX5 and NHX6 (Bassil et al., 2011a). In addition to a notable delay in labeling of the vacuole with the endocytosis tracer FM4-64, *nhx5 nhx6* plants also exhibited a missorting of carboxypeptidase Y to the apoplast and had

significantly reduced cell expansion, plant growth, and high sensitivity to salt, suggesting that vesicular ion/pH homeostasis controlled by NHX5 and NHX6 is critical for key cellular processes (Bassil et al., 2012). The colocalization between the VHA- α 1 subunit of the v-ATPase complex and NHX5 and NHX6 at the TGN lead us to postulate that NHX5 and NHX6 function as H⁺ leaks and, therefore, are critical for maintaining luminal pH homeostasis and for the processing and sorting of cellular cargo (Bassil et al., 2011a, 2012).

Phenotypes of *nhx5 nhx6* Seed

During seed maturation, seed storage proteins are synthesized on the ER and sorted to PSVs, where they accumulate as mature forms following proteolytic processing (Gruis et al., 2004; Otegui et al., 2006). In Arabidopsis, the two most abundant seed storage proteins, 2S albumins and 12S globulins, as well as the protease aleurain, require VSR receptors to traffic to PSVs (Shimada et al., 2003; Zouhar et al., 2010). Processing of the 2S and 12S storage proteins takes place in MVBs before they are delivered into storage vacuoles (Otegui et al., 2006). An examination of the protein storage profile revealed that an accumulation of unprocessed, immature forms of both 2S albumins and 12S globulins persisted in developed *nhx5 nhx6* seeds. The accumulation of cargo precursors would suggest that either a fraction of the precursor proteins never reach the MVB in *nhx5 nhx6* or alterations occur in the proteolytic processing of the precursors due to aberrant endomembrane pH. The fact that the majority of the missorted 2S cargo appears to be unprocessed suggested that they may not have even reached the MVBs. Using the propeptide antibody that specifically recognizes unprocessed 2S albumin precursors (Otegui et al., 2006) to label seed thin sections, we found a significant missorting of the pro forms of 2S albumins to the apoplast of *nhx5 nhx6* seeds. Furthermore, an aggregation of large clusters of vesicles containing these storage protein precursors was also noted in *nhx5 nhx6* embryo cells. Lastly, comparable amounts of mature forms of 2S and 12S accumulated in *nhx5 nhx6* as in wild-type seeds, indicating that processing did occur. Collectively, these results suggest that cargo was likely missorted to the apoplast, at least in part, at a step prior to reaching the MVB/PVC, where processing normally occurs (Otegui et al., 2006). Thus, it is possible that inefficient binding of VSR to storage protein precursors might have caused the failure of cargo to reach PSVs.

nhx5 nhx6 plants share similar phenotypes with trafficking-related mutants such as the *vsr* knockouts (Shimada et al., 2003; Zouhar et al., 2010) and the retromer mutants *vps29* and *vps35* (Shimada et al., 2006; Yamazaki et al., 2008; Kang et al., 2012; Nodzyński et al., 2013), including delayed processing of storage proteins and aberrant sorting to the apoplast. The strikingly similar phenotypes of *vsr*, *vps29*, *vps35*, and *nhx5 nhx6*, together with the increased expression of VSR transcripts as well as the high VSR receptor abundance in mature *nhx5 nhx6* seeds, suggest that receptor-mediated cargo sorting to vacuoles might require homeostatic control of luminal ion and/or pH in the Golgi, the TGN, and/or the PVC. Another trafficking-related mutant that exhibits similar phenotypes to *nhx5 nhx6* is *maigo2* (Li et al., 2006). MAIGO2 is involved in the trafficking of storage proteins from the ER to the Golgi. We attempted to evaluate possible defects in ER trafficking to the Golgi in *nhx5 nhx6* by analyzing *MAIGO2* gene expression. In

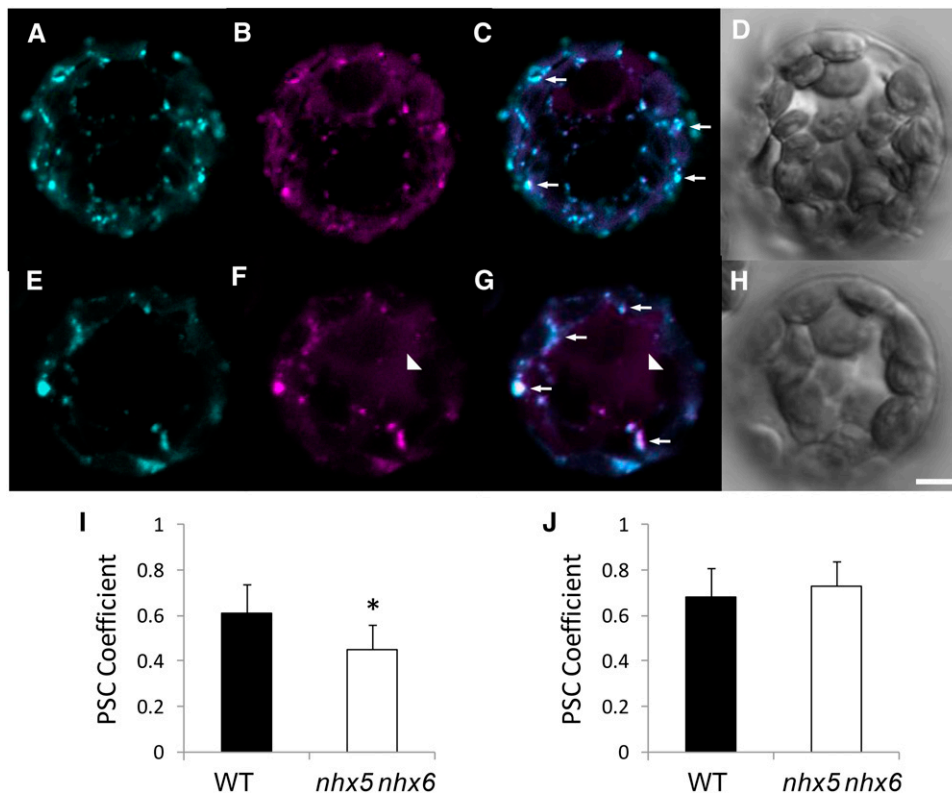


Figure 11. Colocalization of VSR2;1 and Aleurain Is Not Significantly Affected in *nhx5 nhx6* Cells.

(A) to (H) Isolated mesophyll protoplasts of the wild type (A) to (D) and *nhx5 nhx6* (E) to (H) coexpressing VSR2;1-GFP (A) and (E) and Aleu-mRFP (B) and (F). Merged images of VSR2;1-GFP and Aleu-mRFP are shown in (C) and (G). (D) and (H) show differential interference contrast images of the wild type and *nhx5 nhx6*, respectively. Arrowheads indicate diffuse aleurain signal that does not colocalize with VSR2;1. Arrows indicate endosomes in which both fluorescent signals colocalize. Bar = 5 μ m.

(I) Quantification of colocalization between VSR2;1-GFP and Aleu-mRFP in entire protoplasts ($n = 22$ protoplasts). Errors bars indicate sd.

(J) Quantification of colocalization between VSR2;1-GFP and Aleu-mRFP in all endosomes that contain VSR2;1-GFP ($n = 180$ endosomes from 35 protoplasts). The asterisk designates a significant difference between genotypes at $P \leq 0.05$. Errors bars indicate sd.

nhx5 nhx6 seeds at different developmental stages as well as in germinating seedlings, *MAIGO2* expression was similar to that in the wild type. A measure of the quality control of protein synthesis and sorting is the activation of the UPR that occurs in response to an accumulation of unfolded proteins in the ER (Vitale and Ceriotti, 2004). The lectins calreticulin (At1g56340) and the BIP chaperones (BIP1, BIP2, and BIP3) are among the proteins that are rapidly up-regulated at the onset of the UPR (Martínez and Chrispeels, 2003). No differences in the expression of calreticulin or BIP genes were found between the wild type and *nhx5 nhx6*, suggesting that ER function may not have been significantly affected in *nhx5 nhx6* and that the trafficking defects likely occurred downstream of the ER.

NHX5 and NHX6 Are Required for Golgi, TGN, and PVC pH Homeostasis

Given the known functions of NHX-type antiporters (Bassil et al., 2012) as well as direct pH measurements of vacuolar *nhx* mutants (Bassil et al., 2011b), the lack of functional NHX5 and NHX6 should lead to aberrantly acidic luminal pH. We used a set of genetically encoded pHluorin-based pH sensors coupled to VSR2;1 or ST to

target pHluorin to the lumen of either the *trans*-Golgi, TGN, or late PVC (Martinière et al., 2013) and combined pH measurements with colocalization analysis to measure pH in VSR-positive compartments that colocalized with aleurain. We found that the luminal pH was indeed significantly more acidic in *nhx5 nhx6* knockouts (pH 6.1) than in the wild type (pH 6.7). Furthermore, the pH of the Golgi, TGN, and late PVC in *nhx5 nhx6* mutants was also significantly more acidic than in the wild type. In both *nhx5 nhx6* and the wild type, the late PVC remained more alkaline than the TGN and the TGN remained more acidic than the Golgi, similar to what was found in tobacco (*Nicotiana tabacum*) epidermal cells and Arabidopsis root cells (Martinière et al., 2013). The differences among the pH values of the Golgi, TGN, and late PVC are consistent with the localization of NHX5 and NHX6. Previously, we reported that NHX5 highly colocalized with NHX6 and with markers for the Golgi (SYP32) and the TGN (VHAa1) but not with the purported PVC marker SNX1 (Bassil et al., 2011a). Here, we performed additional colocalization analysis in stable expressing lines using the well-characterized markers of the PVC, Rha1 and ARA7, as well as the TGN marker VTI12. NHX5 strongly colocalized with VTI12 but also showed significant colocalization with both ARA7 and Rha1. These

localizations are consistent with the positive response of NHX5 to brefeldin A (Bassil et al., 2011a) as well as to wortmanin (Martinière et al., 2013), and collectively, the results would suggest that NHX5 (and NHX6) may traffic between the Golgi, TGN, and PVC and function in the alkalization of these compartments.

pH- and Receptor-Mediated Protein Trafficking

One current model explaining VSR-mediated transport proposes that the binding of VSR with cargo occurs in the TGN with release at the MVB/PVC (De Marcos Lousa et al., 2012; Robinson et al., 2012). In vitro interaction experiments between a proaleurain peptide and the VSR-like receptor, pea (*Pisum sativum*) BP80, suggested that pH might be critical for the binding and/or release of the receptor with its cargo, because binding occurred at a pH optimum of pH 6.0 and was reduced to half at pH 5.0 or 7.5 (Kirsch et al., 1994; Paris et al., 1997). The hypothesis was postulated that VSRS bind their cargo in the TGN and release them at a more acidic pH in the MVB before recycling back for more cargo binding (Kirsch et al., 1994; Paris et al., 1997; daSilva et al., 2005, 2006). However, this idea is heavily influenced by receptor-ligand interactions in animals, such as the mannose-6-phosphate receptor (Kornfeld, 1992), and relies on the assumption that pH values of equivalent compartments in plants are similar to those in mammalian cells or yeast. Therefore, the characterization of the ionic and pH environment in which receptor-cargo interactions occur (Ahmed et al., 2000; Watanabe et al., 2002) remains paramount for a more complete understanding of receptor-mediated transport.

We evaluated the consequences of aberrant luminal TGN and PVC pH on receptor-mediated cargo by assessing the interaction of VSR with two different cargo proteins, the precursor of 12S globulins (p12S) and the cysteine protease aleurain, using two different methods/approaches. Using 2D BN-PAGE/SDS-PAGE to isolate intact protein complexes, followed by immunodetection of VSR and 12S, we found that a 3-fold reduction in the amount of p12S globulin associated with VSR complexes in *nhx5 nhx6* during seed maturation, suggesting that the binding of VSR receptor with (p12S) cargo was compromised in developing *nhx5 nhx6* seeds. In addition, we used BiFC to test the VSR-aleurain and VSR-12S in vivo interactions and found that significantly less fluorescence complementation occurred in *nhx5 nhx6* cells. The reduction of BiFC in *nhx5 nhx6* was not due to a lower abundance of the partner proteins (VSR or 12S) in BiFC-expressing protoplasts, as shown by the immunodetection of partner protein abundance in BiFC-expressing protoplasts or a consequence of fluorescence quenching due to acidic pH. We ruled out pH-dependent quenching of the green emission signal resulting from fluorescence complementation between super cyan fluorescent protein (C-terminal half; SCYCE) and Venus fluorescent protein (N-terminal half; VYNE) (Gehl et al., 2009) by assessing directly the pH-dependent fluorescence of a chimeric protein, VYNE-SCYCE. Super cyan and Venus fluorescent proteins exhibit stable fluorescence under variable pH or Cl⁻ (Nagai et al., 2002; Kremers et al., 2006). These data, together with the complemented chimera results (this study), suggest that the reduced in vivo interaction between VSR and aleurain/12S was most probably due to a bona fide reduction in VSR and aleurain/12S interactions. A reduction in the VSR and aleurain or VSR and 12S interactions in *nhx5 nhx6* was further supported by

additional experiments in which BiFC between VSR and aleurain in *nhx5 nhx6* was restored to almost wild-type levels when intracellular compartments of *nhx5 nhx6* protoplasts were alkalized to pH 7. Interestingly, when wild-type BiFC protoplasts were acidified, a notable reduction in fluorescence complementation, as a consequence of an acidification-induced VSR-aleurain dissociation, was not observed. This is probably due to the fact that once fluorescence complementation between SCYCE and VYNE complexes occurred, the resulting fluorophore complex remains quite stable or irreversible, as suggested by other BiFC interactions (Kerppola, 2008), and that a dissociation due to low pH would not be possible even if VSR and aleurain themselves dissociated. We ruled out that reduced interaction was a consequence of significant mislocalization of aleurain with VSR by assessing the colocalization between VSR and aleurain. The results indicated that even though some aleurain was mislocalized in *nhx5 nhx6* protoplasts, the aleurain signal associated with VSR vesicles was comparable between *nhx5 nhx6* and the wild type, suggesting that enough partner proteins coexisted in *nhx5 nhx6* to allow for the interaction to occur. Nevertheless, we cannot discard the possibility that the release of the receptor from its cargo might be perturbed in *nhx5 nhx6*, which could indirectly affect receptor-cargo binding. Collectively, our data strongly support the notion that in vivo receptor-cargo interactions are pH dependent.

VSR binding models were proposed before actual pH measurements of compartments of the plant secretory system were obtained (Martinière et al., 2013; Shen et al., 2013). In vivo pH measurements in plant cells revealed that a gradual acidification of pH, ranging from 7.1 in the ER to ~5.5 in the vacuole, exists, similar to that observed in animals (Paroutis et al., 2004), although the existence of alkaline PVC in plants highlights a distinction of the plant endomembrane system (Martinière et al., 2013). Although Shen et al. (2013) reported that the TGN pH was not significantly different from that of the PVC/MVB (~6.2), Martinière et al. (2013) combined TGN- and PVC-specific probes with colocalization to compartment-specific markers to obtain distinct pH values of subpopulations of VSR-labeled TGN and PVC/MVB compartments. Distinct subpopulations of VSR vesicles with unique pH values suggest that pH and VSR receptor-mediated trafficking might be linked. The populations of VSR compartments containing NHX5 were significantly more alkaline than VSR compartments lacking NHX5 or colocalizing with VHAa1. The fact that inhibitors of V-ATPase (concanamycin A) and NHX (amiloride) caused either the respective alkalization or acidification of VSR compartments lends additional support to the importance of both V-ATPase and NHX in maintaining pH in VSR compartments (Martinière et al., 2013). Martinière et al. (2013) also showed that the late PVC is more alkaline (pH 7.1) than the PVC (pH 6.8) or the TGN (pH 6). These pH values correlate well with the localization of NHX5 and V-ATPase (Schumacher and Krebs, 2010). The steep pH gradient between the TGN and PVC is in accordance with the in vitro binding studies and supports the notion that VSR could release its ligand in the PVC, where pH is above the binding optimum, and recycle back to bind more cargo in the TGN, which has a pH closer to the binding optimum (Kirsch et al., 1994). Our data are not at odds with this idea, as the hypothesis would assume that VSR compartments alkalize as they traffic to, or alternatively mature into, the PVC, a role that can be fulfilled by NHX5 and NHX6.

Although our data do not address whether VSR-ligand dissociation could occur in alkaline PVC, they do support the idea that VSR-ligand association would be reduced at aberrantly acidic pH and that the maintenance of VSR-cargo interactions is necessary to ensure the proper delivery of cargo to PSVs. Even though the pH of *nhx5 nhx6* VSR-containing compartments is close to the pH optimum of VSR-ligand binding (determined *in vitro* [Kirsch et al., 1994]), the more acidic luminal pH (measured *in vivo*) in *nhx5 nhx6* compared with the wild type may be too acidic to maintain binding or otherwise promote the release between VSR and the cargo. Alternatively, it is also possible that indirect consequences of pH and/or ionic changes (i.e., K^+ or Ca^{2+}) could contribute to the aberrant VSR-cargo interactions noted in *nhx5 nhx6* cells. Notably, the resulting protein-protein interaction in our BiFC assays probably also resulted in a less dynamic (i.e., more stable or persistent) association of the two binding partners (see above). We evaluated possible consequences of the BiFC interaction to altered localization/trafficking by comparing the localization of BiFC bodies with that of VSR. We found that both BiFC and VSR colocalized to a high degree with the PVC marker ARA7 and less so with Syp61 at the TGN. Importantly, this distribution was not altered in *nhx5 nhx6* cells compared with wild-type cells, suggesting that BiFC may not have significantly altered trafficking or localization. Nonetheless, given the “irreversibility” of BiFC, this method alone is not appropriate to identify the subcellular compartments where receptor-cargo association occurs, and additional experiments (that are beyond the scope of this work) would be performed to identify the true compartment(s) where VSR binding/release occur(s). The sole purpose of using BiFC was to test whether interaction itself is affected by aberrant pH in our *nhx5 nhx6* knockout and not to identify the compartments in which VSR binds its cargo.

In summary, we found that the two vesicular NHX-type antiporters, NHX5 and NHX6, that localize to the Golgi, TGN, and PVC are critical for protein processing and trafficking to the vacuole during seed maturation. *In vivo* pH measurements indicate that the luminal pH of the Golgi, TGN, and PVC, as well as VSR compartments containing its cargo, depend on both antiporters to maintain pH homeostasis; otherwise, they are aberrantly acidic. In these same VSR compartments, we found that VSR binds poorly or does not maintain an association with its cargo and conclude that NHX5- and NHX6-dependent pH regulation is critical for proper receptor-mediated trafficking to the vacuole. Thus, this work presents an *in vivo* demonstration of the importance of pH-dependent receptor-cargo interaction in protein trafficking.

METHODS

Plant Material and Growth Conditions

Arabidopsis thaliana wild type (ecotype Columbia-0) and T-DNA insertion knockouts were obtained from the ABRC and described previously [Bassil et al., 2011a]. Plants were grown in Sunshine Mix 4 (SunGro) at 22°C under diurnal light conditions (8 h of light and 16 h of dark).

Seed Protein Isolation and Immunoblots

For extraction of proteins, dry, 3-d and 6-d germinated seeds (60 each) of *Arabidopsis* Columbia-0 and F37 (*nhx5 nhx6* double mutant) were homogenized in 150 μ L of extraction buffer, pH 7.5, containing 25 mM Tris-HCl, 2

mM $MgCl_2$, 250 mM sucrose, 1 mM DTT, and a protease inhibitor mix (Sigma-Aldrich). The homogenate was centrifuged at 15,000g for 2 min at 4°C, and the protein concentration was determined in the supernatant using a Bradford assay [Bradford, 1976]. Samples were diluted (63 mM Tris, 10% glycerol, 2% SDS, 5% mercaptoethanol, and 0.01% bromophenol blue, pH 6.8) to 10 μ g of protein, heated to 95°C for 5 min, and centrifuged at 15,000g for 2 min. The supernatant was resolved with SDS-PAGE (10%) in Laemmli buffer [Laemmli, 1970]. For immunoblots, gels were immediately transferred onto polyvinylidene difluoride membranes using a wet-blot tank system with a constant voltage (100 V), briefly rinsed in Tris-buffered saline solution (50 mM Tris and 200 mM NaCl, pH 7.5), blocked in 5% blocking solution (Amersham), and incubated overnight at 4°C with primary antibodies at the following dilutions: anti-12S globulin α -subunit, 1:10,000; anti-2S albumin, 1:10,000 [Shimada et al., 2003]; anti-VSR, 1:5000 [Yamada et al., 2005]; and anti-GFP, 1:1000 (Novus Biologicals). Immunoreactive polypeptides were visualized using a horseradish peroxidase-conjugated secondary antibody (1:10,000) and ECL detection (Pierce).

BN-PAGE

Protein samples were extracted from developing seeds of wild-type and *nhx5 nhx6* siliques by using the protocol described by Wittig et al. (2006). The extraction buffer (50 mM NaCl, 50 mM imidazole-HCl, 2 mM 6-aminohexanoic acid, 1 mM EDTA, and 400 mM sucrose, pH 7) was used to preserve multiprotein complexes upon freezing. 2D BN-PAGE was performed as suggested by the manufacturer (Invitrogen NativePAGE Novex Bis-Tris Gel System).

For 2D analysis, a single lane from 1D BN-PAGE was cut out from the gel, denatured with 1% SDS and 2% β -mercaptoethanol, and resolved in the second dimension on an SDS polyacrylamide gel prior to immunoblotting. Blots were stripped and reprobed following a harsh stripping method. Stripping buffer composition was 2% SDS, 62.5 mM Tris-HCl, pH 6.8, and 0.8% β -mercaptoethanol. Membranes were incubated at 55°C for 45 min followed by three 10-min washes with water. Immunoblotting was then performed as described above. For the quantification of relative signals of VSR1 and 12S on blots from 2D BN-PAGE/SDS-PAGE, wild-type and *nhx5 nhx6* films were exposed and scanned identically. We quantified pixel intensity and area as described in Results and outlined in Supplemental Figure 5 using ImageJ (<http://rsbweb.nih.gov/ij/>) in each of four replicates of the experiment. In order to quantify and compare the relative abundance of VSR and p12S in wild-type and *nhx5 nhx6* complexes, we estimated the amount of signal in each spot (spot intensity multiplied by spot area delineated by ovals; Supplemental Figure 6) by identifying the portions of VSR and p12S that overlap in wild-type of *nhx5 nhx6* complexes. Because the same membranes were used for the VSR and 12S blots, we could identify the exact position of each VSR and p12S spot in the complexes (see vertical bounding lines in Supplemental Figure 6). For each antibody, the same exposure time and scanning settings of wild-type and *nhx5 nhx6* blots were used, and four independent replicates were quantified.

Constructs

For the BiFC experiments, the N-terminal half of VENUS (VYNE) and the C-terminal half of super cyan fluorescent protein (SCYCE) were used, which result in a 515-nm emission when fluorescence complementation occurs [Gehl et al., 2009]. For the Aleu-VYNE, a 420-bp cDNA fragment from the start codon of aleurain At5g60360 was cloned into pDONR207 (Invitrogen) to generate an entry vector, pENTR-Aleu, and recombined into pDEST-G^WVYNE and pDEST-G^WSCYNE [Gehl et al., 2009]. We used the first 140 amino acids of aleurain, which includes the signal sequence and the N-terminal propeptide, based on the barley (*Hordeum vulgare*) construct described previously by Di Sansebastiano et al. (2001). Full-length cDNA encoding *Arabidopsis* 12S (CRU1) At5g44120 lacking a stop codon was cloned into pDONR207 to generate an entry vector, pENTR-12S, and recombined into pDEST-G^WVYNE, resulting in 12S-VYNE. The SCYCE-VSR2;1

(VSR2;1-At2g14720) construct was generated based on the pHluorin-VSR construct (Martinière et al., 2013). Signal peptide (SP)-VYNE and SP-SCYCE fragments were amplified from pDEST-VYNE(R)^{GW} and pDEST-SCYCE(R)^{GW} (Gehl et al., 2009), respectively, and inserted between XbaI and SpeI sites of pH-VSR to generate SCYCE-VSR2;1 (Supplemental Tables 1 and 2). pH-VSR, pH-VSR-Y (TGN), and pH-VSR-IM (PVC) used for the measurement of luminal pH were described previously by Martinière et al. (2013). For the VYNE and SCYCE chimera proteins, overlapping PCR was performed. A VYNE fragment was amplified with B1-GFP and VYNEr primers from pDEST-VYNE(R)^{GW}. A SCYCE fragment was amplified with SCYCEf and B2-GFP primers from pDEST-^{GW}SCYNE. Both fragments were purified and used as templates for a second PCR using primers B1-GFP and B2-GFP to produce the chimera VYNE+SCYCE, introduced in pDONR207 to generate an entry vector, pENTR-chimera, and recombined into pEarleyGate100 (Earley et al., 2006). PIP2;1-GFP was described by Boursiac et al. (2005). Aleu-mRFP was generated using the same entry vector used for the Aleu-VYNE (pENTR-Aleu), except that it was recombined into pH7RWG 2.0 (Karimi et al., 2007). VSR1-mRFP was a kind gift from J.C. Rogers (Park et al., 2007), and PIP2;1-GFP was a gift from C. Maurel (Boursiac et al., 2005).

Transient Expression in Isolated Protoplasts

Protoplast transient transformation was performed using Arabidopsis mesophyll cells following the protocol described by Yoo et al. (2007). Four-week-old plants grown in 8 h of light were used for protoplast isolation. Protoplasts were visualized 18 h after transformation.

Confocal Laser Scanning Microscopy

Fluorescent images were acquired using a Zeiss LSM 710 confocal microscope equipped with a 63× objective, using sequential line scanning mode with settings described previously (Bassil et al., 2011a; Martinière et al., 2013). For the measurement of vesicle pH, the emission (500 to 550 nm) of pHluorin was used to calculate a ratio, following sequential excitation with 488- and 405-nm lasers, and used to calculate the pH using the calibration curve (Figure 6B). In vivo calibration was performed on a subset of the same protoplasts used for pH measurements at the end of each experiment. Protoplasts were incubated in WI protoplast buffer (0.5 M mannitol and 20 mM KCl; Yoo et al., 2007) with 25 μM nigericin, 60 mM KCl, and 10 mM MES/HEPES Bis-Tris-propane adjusted to different pH values ranging from 5 to 8 for each calibration point. Fluorescence ratio imaging was performed 5 min after incubation. The ratio was used to calculate the pH from the calibration curve and represented visually by pseudocoloring images. The measurement of the luminal pH of the Golgi, TGN, and PVC was done using the compartment-specific probes ST-pH, pH-VSR-Y (TGN), and pH-VSR-IM (PVC) as described previously (Martinière et al., 2013).

For BiFC experiments, green emission (500 to 550 nm) and mRFP (585 to 620 nm) were collected following excitation with 488- and 561-nm lasers. A comparative analysis of images between *nhx5 nhx6* and the wild type was possible because the same laser intensity, gain, line averaging, and image processing were used. For quantification of the number of BiFC bodies, a z-stack of five sections, ranging from 1- to 2.5-μm-thick sections from similarly sized protoplasts, was used to create 3D reconstructed images. In order not to bias the number of vesicles that were imaged (and counted), the approach used was identical in both wild-type and *nhx5 nhx6* protoplasts. From each of 25 3D unthresholded protoplast images derived from three independent experiments, we summed the pixel intensities of the VSR1-mRFP and BiFC-green signals in regions of interest surrounding each vesicle and normalized the green emission to that of RFP, in order to obtain a ratio for each vesicle in wild-type and *nhx5 nhx6* protoplasts. Postacquisition image processing was done with the Zen Zeiss software (2011) and ImageJ (version 1.45d). Colocalization analysis was performed as described previously (Bassil et al., 2011a; Martinière et al., 2013) and using the Fiji plugin coloc2 (http://fiji.sc/Coloc_2).

Electron Microscopy

Dry seeds were cut and fixed in 4% (w/v) paraformaldehyde, 1% (v/v) glutaraldehyde, 0.05 M cacodylate buffer, pH 7.4, and 10% DMSO. Ultrathin sections were incubated with primary antibodies against Arabidopsis 2S albumin (1:50), Arabidopsis 12S globulin α-subunit (1:50) (Shimada et al., 2003), Arabidopsis N-terminal p2S, and Arabidopsis internal peptide p2S (Otegui et al., 2006), followed by incubation with 10-nm gold-coupled secondary antibody, and examined as described previously (Bassil et al., 2011b).

For the analysis of the endomembrane system, developing embryos were high-pressure frozen, freeze-substituted, and immunogold-labeled as explained by Otegui et al. (2006). The anti-VSR antibody was a gift from Ikuko Hara-Nishimura (Kyoto University) and was diluted 1:10 (Shimada et al., 2006). For the quantification of immunolocalized gold particles, three fields from each of 10 sections having five to seven cells was used.

Quantitative PCR Analysis

RNA was extracted from seeds and germinated seedlings with six biological replicates. Approximately 60 to 80 seeds were dissected, and around 50 seedlings were collected, ground in liquid N, and homogenized using the PureLink Plant RNA Reagent (Invitrogen). RNA extraction was performed following manufacturer instructions. First-strand cDNA was synthesized from 1 μg of total RNA with the QuantiTect Reverse Transcription kit (Qiagen). Primer Express software (Applied Biosystems) was used for primer design. Quantitative real-time PCR was performed as described before (Bassil et al., 2011a). The primers used for the amplification of the target genes are listed in Supplemental Table 3.

Accession Numbers

Sequence data from this article can be found in the Arabidopsis Genome Initiative or GenBank/EMBL databases under the following accession numbers: VSR1 (VSR1;1), At3g52850; VSR2;1 (VSR4), At2g14720; NHX5, At1g54370; NHX6, At1g79610; 12S globulin, At5g44120; 2S albumin, At4g27140, At4g27150, At4g27160; aleurain, At3g45310; ARA7, At4g19640; Rha1 At5g45130; VT112, At1g26670.

Supplemental Data

Supplemental Figure 1. Quantitative real-time PCR of storage protein expression.

Supplemental Figure 2. Transmission electron micrographs of dry seed thin sections.

Supplemental Figure 3. Quantitative real-time PCR of three unfolded protein response genes.

Supplemental Figure 4. Immunogold localization and quantification of VSR in seed embryos.

Supplemental Figure 5. Immunodetection of VSR1 protein abundance and quantitative real-time PCR of VSR1 expression.

Supplemental Figure 6. Loading controls and identification and quantification of native complexes using 2D blue-native SDS-PAGE.

Supplemental Figure 7. Transient expression and quantification of VSR1-mRFP.

Supplemental Figure 8. In vivo interaction of VSR2;1 and 12S globulin.

Supplemental Figure 9. Abundance of bimolecular fluorescence complementation partner proteins.

Supplemental Figure 10. Colocalization of bimolecular fluorescence complementation bodies and VSR.

Supplemental Table 1. Constructs used for bimolecular fluorescence complementation experiments.

Supplemental Table 2. List of primers used to generate constructs used for bimolecular fluorescence complementation experiments.

Supplemental Table 3. List of primers used for quantitative real-time PCR.

ACKNOWLEDGMENTS

We thank J.C. Rogers for constructs and discussion, Ikuko-Hara Nishimura for antibodies, Christophe Maurel for constructs, and Arsenio Villarejo for many stimulating discussions. We thank the Salk Institute Genomic Analysis Laboratory for generating the sequence-indexed *Arabidopsis nhx5 nhx6* T-DNA insertional mutants and the ABRC for providing them. This work was supported in part by the National Science Foundation (Grants MCB-0343279 and IOS-0820112 to E. Blumwald and Grant MCB1157824 to M.S.O.) and the Will W. Lester Endowment, University of California (to E. Blumwald).

AUTHOR CONTRIBUTIONS

M.R., E. Bassil, H.T., M.S.O., N.P., and E. Blumwald designed the experiments. M.R., E. Bassil, H.T., M.W., and A.C. carried out experiments. M.R., E. Bassil, and E. Blumwald wrote the article.

Received December 19, 2014; revised February 26, 2015; accepted March 12, 2015; published March 31, 2015.

REFERENCES

- Ahmed, S.U., Rojo, E., Kovaleva, V., Venkataraman, S., Dombrowski, J.E., Matsuo, K., and Raikhel, N.V. (2000). The plant vacuolar sorting receptor AtELP is involved in transport of NH₂-terminal propeptide-containing vacuolar proteins in *Arabidopsis thaliana*. *J. Cell Biol.* **149**: 1335–1344.
- Apse, M.P., Aharon, G.S., Snedden, W.A., and Blumwald, E. (1999). Salt tolerance conferred by overexpression of a vacuolar Na⁺/H⁺ antiporter in *Arabidopsis*. *Science* **285**: 1256–1258.
- Apse, M.P., Sottosanto, J.B., and Blumwald, E. (2003). Vacuolar cation/H⁺ exchange, ion homeostasis, and leaf development are altered in a T-DNA insertional mutant of AtNHX1, the *Arabidopsis* vacuolar Na⁺/H⁺ antiporter. *Plant J.* **36**: 229–239.
- Barragán, V., Leidi, E.O., Andrés, Z., Rubio, L., De Luca, A., Fernández, J.A., Cubero, B., and Pardo, J.M. (2012). Ion exchangers NHX1 and NHX2 mediate active potassium uptake into vacuoles to regulate cell turgor and stomatal function in *Arabidopsis*. *Plant Cell* **24**: 1127–1142.
- Bassil, E., and Blumwald, E. (2014). The ins and outs of intracellular ion homeostasis: NHX-type cation/H⁺ transporters. *Curr. Opin. Plant Biol.* **22**: 1–6.
- Bassil, E., Coku, A., and Blumwald, E. (2012). Cellular ion homeostasis: Emerging roles of intracellular NHX Na⁺/H⁺ antiporters in plant growth and development. *J. Exp. Bot.* **63**: 5727–5740.
- Bassil, E., Ohto, M.A., Esumi, T., Tajima, H., Zhu, Z., Cagnac, O., Belmonte, M., Peleg, Z., Yamaguchi, T., and Blumwald, E. (2011a). The *Arabidopsis* intracellular Na⁺/H⁺ antiporters NHX5 and NHX6 are endosome associated and necessary for plant growth and development. *Plant Cell* **23**: 224–239.
- Bassil, E., Tajima, H., Liang, Y.-C., Ohto, M.A., Ushijima, K., Nakano, R., Esumi, T., Coku, A., Belmonte, M., and Blumwald, E. (2011b). The *Arabidopsis* Na⁺/H⁺ antiporters NHX1 and NHX2 control vacuolar pH and K⁺ homeostasis to regulate growth, flower development, and reproduction. *Plant Cell* **23**: 3482–3497.
- Blumwald, E. (1987). Tonoplast vesicles as a tool in the study of ion-transport at the plant vacuole. *Physiol. Plant.* **69**: 731–734.
- Boursiac, Y., Chen, S., Luu, D.T., Sorieul, M., van den Dries, N., and Maurel, C. (2005). Early effects of salinity on water transport in *Arabidopsis* roots. Molecular and cellular features of aquaporin expression. *Plant Physiol.* **139**: 790–805.
- Bowers, K., Levi, B.P., Patel, F.I., and Stevens, T.H. (2000). The sodium/proton exchanger Nhx1p is required for endosomal protein trafficking in the yeast *Saccharomyces cerevisiae*. *Mol. Biol. Cell* **11**: 4277–4294.
- Bradford, M.M. (1976). A rapid and sensitive method for the quantitation of microgram quantities of protein utilizing the principle of protein-dye binding. *Anal. Biochem.* **72**: 248–254.
- Brett, C.L., Tukaye, D.N., Mukherjee, S., and Rao, R. (2005). The yeast endosomal Na⁺K⁺/H⁺ exchanger Nhx1 regulates cellular pH to control vesicle trafficking. *Mol. Biol. Cell* **16**: 1396–1405.
- Brüx, A., Liu, T.Y., Krebs, M., Stierhof, Y.D., Lohmann, J.U., Miersch, O., Wasternack, C., and Schumacher, K. (2008). Reduced V-ATPase activity in the *trans*-Golgi network causes oxylipin-dependent hypocotyl growth inhibition in *Arabidopsis*. *Plant Cell* **20**: 1088–1100.
- Casey, J.R., Grinstein, S., and Orlowski, J. (2010). Sensors and regulators of intracellular pH. *Nat. Rev. Mol. Cell Biol.* **11**: 50–61.
- Chanroj, S., Wang, G., Venema, K., Zhang, M.W., Delwiche, C.F., and Sze, H. (2012). Conserved and diversified gene families of monovalent cation/H⁺ antiporters from algae to flowering plants. *Front. Plant Sci.* **3**: 25.
- Craddock, C.P., Hunter, P.R., Szakacs, E., Hinz, G., Robinson, D.G., and Frigerio, L. (2008). Lack of a vacuolar sorting receptor leads to non-specific missorting of soluble vacuolar proteins in *Arabidopsis* seeds. *Traffic* **9**: 408–416.
- daSilva, L.L., Foresti, O., and Denecke, J. (2006). Targeting of the plant vacuolar sorting receptor BP80 is dependent on multiple sorting signals in the cytosolic tail. *Plant Cell* **18**: 1477–1497.
- daSilva, L.L., Taylor, J.P., Hadlington, J.L., Hanton, S.L., Snowden, C.J., Fox, S.J., Foresti, O., Brandizzi, F., and Denecke, J. (2005). Receptor salvage from the prevacuolar compartment is essential for efficient vacuolar protein targeting. *Plant Cell* **17**: 132–148.
- De Marcos Lousa, C., Gershlick, D.C., and Denecke, J. (2012). Mechanisms and concepts paving the way towards a complete transport cycle of plant vacuolar sorting receptors. *Plant Cell* **24**: 1714–1732.
- Detmer, J., Hong-Hermesdorf, A., Stierhof, Y.D., and Schumacher, K. (2006). Vacuolar H⁺-ATPase activity is required for endocytic and secretory trafficking in *Arabidopsis*. *Plant Cell* **18**: 715–730.
- Di Sansebastiano, G.P., Paris, N., Marc-Martin, S., and Neuhaus, J.-M. (2001). Regeneration of a lytic central vacuole and of neutral peripheral vacuoles can be visualized by green fluorescent proteins targeted to either type of vacuoles. *Plant Physiol.* **126**: 78–86.
- Earley, K.W., Haag, J.R., Pontes, O., Opper, K., Juehne, T., Song, K., and Pikaard, C.S. (2006). Gateway-compatible vectors for plant functional genomics and proteomics. *Plant J.* **45**: 616–629.
- Foresti, O., and Denecke, J. (2008). Intermediate organelles of the plant secretory pathway: Identity and function. *Traffic* **9**: 1599–1612.
- Fujiwara, T., Nambara, E., Yamagishi, K., Goto, D.B., and Naito, S. (2002). Storage proteins. *The Arabidopsis Book* **1**: e0020, doi/10.1199/tab.0020.

- Gehl, C., Waadt, R., Kudla, J., Mendel, R.-R., and Hänsch, R. (2009). New GATEWAY vectors for high throughput analyses of protein-protein interactions by bimolecular fluorescence complementation. *Mol. Plant* **2**: 1051–1058.
- Geldner, N., Dénervaud-Tendon, V., Hyman, D.L., Mayer, U., Stierhof, Y.D., and Chory, J. (2009). Rapid, combinatorial analysis of membrane compartments in intact plants with a multicolor marker set. *Plant J.* **59**: 169–178.
- Gruis, D., Schulze, J., and Jung, R. (2004). Storage protein accumulation in the absence of the vacuolar processing enzyme family of cysteine proteases. *Plant Cell* **16**: 270–290.
- Hara-Nishimura, I., Shimada, T., Hatano, K., Takeuchi, Y., and Nishimura, M. (1998). Transport of storage proteins to protein storage vacuoles is mediated by large precursor-accumulating vesicles. *Plant Cell* **10**: 825–836.
- Hu, C.-D., Chinenov, Y., and Kerppola, T.K. (2002). Visualization of interactions among bZIP and Rel family proteins in living cells using bimolecular fluorescence complementation. *Mol. Cell* **9**: 789–798.
- Kang, H., Kim, S.Y., Song, K., Sohn, E.J., Lee, Y., Lee, D.W., Hara-Nishimura, I., and Hwang, I. (2012). Trafficking of vacuolar proteins: The crucial role of *Arabidopsis* vacuolar protein sorting 29 in recycling vacuolar sorting receptor. *Plant Cell* **24**: 5058–5073.
- Karimi, M., Depicker, A., and Hilson, P. (2007). Recombinational cloning with plant Gateway vectors. *Plant Physiol.* **145**: 1144–1154.
- Kerppola, T.K. (2008). Bimolecular fluorescence complementation (BiFC) analysis as a probe of protein interactions in living cells. *Annu. Rev. Biophys.* **37**: 465–487.
- Kim, H., Kang, H., Jang, M., Chang, J.H., Miao, Y., Jiang, L., and Hwang, I. (2010). Homomeric interaction of AtVSR1 is essential for its function as a vacuolar sorting receptor. *Plant Physiol.* **154**: 134–148.
- Kim, J.H., Lingwood, C.A., Williams, D.B., Furuya, W., Manolson, M.F., and Grinstein, S. (1996). Dynamic measurement of the pH of the Golgi complex in living cells using retrograde transport of the verotoxin receptor. *J. Cell Biol.* **134**: 1387–1399.
- Kirsch, T., Paris, N., Butler, J.M., Beevers, L., and Rogers, J.C. (1994). Purification and initial characterization of a potential plant vacuolar targeting receptor. *Proc. Natl. Acad. Sci. USA* **91**: 3403–3407.
- Kneen, M., Farinas, J., Li, Y., and Verkman, A.S. (1998). Green fluorescent protein as a noninvasive intracellular pH indicator. *Biophys. J.* **74**: 1591–1599.
- Kornfeld, S. (1992). Structure and function of the mannose 6-phosphate/insulinlike growth factor II receptors. *Annu. Rev. Biochem.* **61**: 307–330.
- Kremers, G.-J., Goedhart, J., van Munster, E.B., and Gadella, T.W.J., Jr. (2006). Cyan and yellow super fluorescent proteins with improved brightness, protein folding, and FRET Förster radius. *Biochemistry* **45**: 6570–6580.
- Laemmli, U.K. (1970). Cleavage of structural proteins during the assembly of the head of bacteriophage T4. *Nature* **227**: 680–685.
- Lam, S.K., Siu, C.L., Hillmer, S., Jang, S., An, G., Robinson, D.G., and Jiang, L. (2007). Rice SCAMP1 defines clathrin-coated, trans-Golgi-located tubular-vesicular structures as an early endosome in tobacco BY-2 cells. *Plant Cell* **19**: 296–319.
- Li, L., Shimada, T., Takahashi, H., Ueda, H., Fukao, Y., Kondo, M., Nishimura, M., and Hara-Nishimura, I. (2006). MAIG2 is involved in exit of seed storage proteins from the endoplasmic reticulum in *Arabidopsis thaliana*. *Plant Cell* **18**: 3535–3547.
- Martínez, I.M., and Chrispeels, M.J. (2003). Genomic analysis of the unfolded protein response in *Arabidopsis* shows its connection to important cellular processes. *Plant Cell* **15**: 561–576.
- Martinière, A., Bassil, E., Jublanc, E., Alcon, C., Reguera, M., Sentenac, H., Blumwald, E., and Paris, N. (2013). In vivo intracellular pH measurements in tobacco and *Arabidopsis* reveal an unexpected pH gradient in the endomembrane system. *Plant Cell* **25**: 4028–4043.
- Matsuoka, K., Higuchi, T., Maeshima, M., and Nakamura, K. (1997). A vacuolar-type H⁺-ATPase in a nonvacuolar organelle is required for the sorting of soluble vacuolar protein precursors in tobacco cells. *Plant Cell* **9**: 533–546.
- Miao, Y., Li, K.Y., Li, H.Y., Yao, X., and Jiang, L. (2008). The vacuolar transport of aleurain-GFP and 2S albumin-GFP fusions is mediated by the same pre-vacuolar compartments in tobacco BY-2 and *Arabidopsis* suspension cultured cells. *Plant J.* **56**: 824–839.
- Nagai, T., Ibata, K., Park, E.S., Kubota, M., Mikoshiba, K., and Miyawaki, A. (2002). A variant of yellow fluorescent protein with fast and efficient maturation for cell-biological applications. *Nat. Biotechnol.* **20**: 87–90.
- Nielsen, E., Cheung, A.Y., and Ueda, T. (2008). The regulatory RAB and ARF GTPases for vesicular trafficking. *Plant Physiol.* **147**: 1516–1526.
- Nodzyński, T., Feraru, M.I., Hirsch, S., De Rycke, R., Niculaes, C., Boerjan, W., Van Leene, J., De Jaeger, G., Vanneste, S., and Friml, J. (2013). Retromer subunits VPS35A and VPS29 mediate prevacuolar compartment (PVC) function in *Arabidopsis*. *Mol. Plant* **6**: 1849–1862.
- Ohgaki, R., van IJendoorn, S.C.D., Matsushita, M., Hoekstra, D., and Kanazawa, H. (2011). Organellar Na⁺/H⁺ exchangers: Novel players in organelle pH regulation and their emerging functions. *Biochemistry* **50**: 443–450.
- Orlowski, J., and Grinstein, S. (2011). Na⁺/H⁺ exchangers. *Compr. Physiol.* **1**: 2083–2100.
- Otegui, M.S., Herder, R., Schulze, J., Jung, R., and Staehelin, L.A. (2006). The proteolytic processing of seed storage proteins in *Arabidopsis* embryo cells starts in the multivesicular bodies. *Plant Cell* **18**: 2567–2581.
- Paris, N., Rogers, S.W., Jiang, L., Kirsch, T., Beevers, L., Phillips, T.E., and Rogers, J.C. (1997). Molecular cloning and further characterization of a probable plant vacuolar sorting receptor. *Plant Physiol.* **115**: 29–39.
- Park, J.H., Oufattole, M., and Rogers, J.C. (2007). Golgi-mediated vacuolar sorting in plant cells: RMR proteins are sorting receptors for the protein aggregation/membrane internalization pathway. *Plant Sci.* **172**: 728–745.
- Paroutis, P., Touret, N., and Grinstein, S. (2004). The pH of the secretory pathway: Measurement, determinants, and regulation. *Physiology (Bethesda)* **19**: 207–215.
- Rea, P.A., and Poole, R.J. (1993). Vacuolar H⁺-translocating pyrophosphatase. *Annu. Rev. Plant Physiol. Plant Mol. Biol.* **44**: 157–180.
- Reyes, F.C., Buono, R., and Otegui, M.S. (2011). Plant endosomal trafficking pathways. *Curr. Opin. Plant Biol.* **14**: 666–673.
- Robinson, D.G., Pimpl, P., Scheuring, D., Stierhof, Y.-D., Sturm, S., and Viotti, C. (2012). Trying to make sense of retromer. *Trends Plant Sci.* **17**: 431–439.
- Rodríguez-Rosales, M.P., Gálvez, F.J., Huertas, R., Aranda, M.N., Baghour, M., Cagnac, O., and Venema, K. (2009). Plant NHX cation/proton antiporters. *Plant Signal. Behav.* **4**: 265–276.
- Saint-Jean, B., Seveno-Carpentier, E., Alcon, C., Neuhaus, J.-M., and Paris, N. (2010). The cytosolic tail dipeptide Ile-Met of the pea receptor BP80 is required for recycling from the prevacuole and for endocytosis. *Plant Cell* **22**: 2825–2837.
- Saint-Jore-Dupas, C., Nebenführ, A., Boulaflois, A., Follet-Gueye, M.-L., Plasson, C., Hawes, C., Driouch, A., Faye, L., and Gomord, V. (2006). Plant N-glycan processing enzymes employ different targeting mechanisms for their spatial arrangement along the secretory pathway. *Plant Cell* **18**: 3182–3200.

- Sanmartín, M., Ordóñez, A., Sohn, E.J., Robert, S., Sánchez-Serrano, J.J., Surpin, M.A., Raikhel, N.V., and Rojo, E.** (2007). Divergent functions of VT112 and VT111 in trafficking to storage and lytic vacuoles in *Arabidopsis*. *Proc. Natl. Acad. Sci. USA* **104**: 3645–3650.
- Scheuring, D., Viotti, C., Krüger, F., Künzl, F., Sturm, S., Bubeck, J., Hillmer, S., Frigerio, L., Robinson, D., Pimpl, P., and Schumacher, K.** (2011). Multivesicular bodies mature from the trans-Golgi network/early endosome in *Arabidopsis*. *Plant Cell* **23**: 3463–3481.
- Schumacher, K.** (2014). pH in the plant endomembrane system—An import and export business. *Curr. Opin. Plant Biol.* **22**: 71–76.
- Schumacher, K., and Krebs, M.** (2010). The V-ATPase: Small cargo, large effects. *Curr. Opin. Plant Biol.* **13**: 724–730.
- Shen, J., Zeng, Y., Zhuang, X., Sun, L., Yao, X., Pimpl, P., and Jiang, L.** (2013). Organelle pH in the *Arabidopsis* endomembrane system. *Mol. Plant* **6**: 1419–1437.
- Shimada, T., Fuji, K., Tamura, K., Kondo, M., Nishimura, M., and Hara-Nishimura, I.** (2003). Vacuolar sorting receptor for seed storage proteins in *Arabidopsis thaliana*. *Proc. Natl. Acad. Sci. USA* **100**: 16095–16100.
- Shimada, T., Koumoto, Y., Li, L., Yamazaki, M., Kondo, M., Nishimura, M., and Hara-Nishimura, I.** (2006). AtVPS29, a putative component of a retromer complex, is required for the efficient sorting of seed storage proteins. *Plant Cell Physiol.* **47**: 1187–1194.
- Toyooka, K., Goto, Y., Asatsuma, S., Koizumi, M., Mitsui, T., and Matsuoka, K.** (2009). A mobile secretory vesicle cluster involved in mass transport from the Golgi to the plant cell exterior. *Plant Cell* **21**: 1212–1229.
- Viotti, C., et al.** (2010). Endocytic and secretory traffic in *Arabidopsis* merge in the trans-Golgi network/early endosome, an independent and highly dynamic organelle. *Plant Cell* **22**: 1344–1357.
- Vitale, A., and Ceriotti, A.** (2004). Protein quality control mechanisms and protein storage in the endoplasmic reticulum. A conflict of interests? *Plant Physiol.* **136**: 3420–3426.
- Watanabe, E., Shimada, T., Kuroyanagi, M., Nishimura, M., and Hara-Nishimura, I.** (2002). Calcium-mediated association of a putative vacuolar sorting receptor PV72 with a propeptide of 2S albumin. *J. Biol. Chem.* **277**: 8708–8715.
- Wittig, I., Braun, H.-P., and Schägger, H.** (2006). Blue native PAGE. *Nat. Protoc.* **1**: 418–428.
- Yamada, K., Fuji, K., Shimada, T., Nishimura, M., and Hara-Nishimura, I.** (2005). Endosomal proteases facilitate the fusion of endosomes with vacuoles at the final step of the endocytotic pathway. *Plant J.* **41**: 888–898.
- Yamazaki, M., Shimada, T., Takahashi, H., Tamura, K., Kondo, M., Nishimura, M., and Hara-Nishimura, I.** (2008). *Arabidopsis* VPS35, a retromer component, is required for vacuolar protein sorting and involved in plant growth and leaf senescence. *Plant Cell Physiol.* **49**: 142–156.
- Yoo, S.-D., Cho, Y.-H., and Sheen, J.** (2007). *Arabidopsis* mesophyll protoplasts: A versatile cell system for transient gene expression analysis. *Nat. Protoc.* **2**: 1565–1572.
- Yoshida, K., Kondo, T., Okazaki, Y., and Katou, K.** (1995). Cause of blue petal color. *Nature* **373**: 291.
- Zouhar, J., Muñoz, A., and Rojo, E.** (2010). Functional specialization within the vacuolar sorting receptor family: VSR1, VSR3 and VSR4 sort vacuolar storage cargo in seeds and vegetative tissues. *Plant J.* **64**: 577–588.